Economic Geology, v. 111, pp. 127–150

Age and Geologic Setting of Quartz Vein-Hosted Gold Mineralization at Curraghinalt, Northern Ireland: Implications for Genesis and Classification*

C. M. Rice,[1,†] D. F. Mark,[2] D. Selby,[3] J. E. Neilson,[1] and B. Davidheiser-Kroll[2]

[1] *Department of Geology and Petroleum Geology, University of Aberdeen, Aberdeen AB24 3UE, United Kingdom*

[2] *Isotope Geosciences Unit, Scottish Environmental Research Centre (SUERC), Rankine Avenue, East Kilbride G75 0QF, United Kingdom*

[3] *Department of Earth Sciences, University of Durham, Durham DH1 3LE, United Kingdom*

Abstract

The Caledonian orogenic belt of northern Britain hosts some significant quartz vein-hosted gold deposits. However, as in orogenic belts worldwide, the relationship between gold mineralization and regional tectonics, magmatism, and metamorphism is a matter of debate. This is primarily due to the absence of precise temporal constraints for the mineralization. Here we report high-precision $^{40}Ar/^{39}Ar$ and Re-Os ages for the largest known gold deposit at Curraghinalt (2.7 Moz) in Northern Ireland and use these ages to constrain the regional geologic setting of the gold mineralization and establish a genetic model.

The gold resource is contained in a suite of quartz sulfide veins hosted by Neoproterozoic (Dalradian) metasediments, which have been thrust over an Ordovician island arc (Tyrone Igneous Complex). Previous studies recognized two generations of gold sulfide mineralization and we have identified a third in microshears that cut the veins. In the absence of precise geochronological data, mineralization ages from Ordovician to Carboniferous have been proposed.

We have dated muscovite ($^{40}Ar/^{39}Ar$) in quartz vein-hosted clasts of Dalradian wall rock to 459.3 ± 3.4 Ma (all $^{40}Ar/^{39}Ar$ and Re-Os ages herein are reported at the 2σ confidence level including all sources of uncertainty), an age that we interpret as representing the regional cooling path and which provides a maximum age constraint for all gold mineralization. This is consistent with the quartz veins postdating the end of main-stage deformation in the Grampian event of the Caledonian orogeny (ca. 465 Ma).

Molybdenite (Re-Os) and sericite ($^{40}Ar/^{39}Ar$) from the newly identified gold-bearing microshears (third generation of gold mineralization) yield indistinguishable Re-Os models and $^{40}Ar/^{39}Ar$ ages, with a combined age of 455.8 ± 3.0 Ma. The radioisotope ages and field evidence temporally constrain gold mineralization at Curraghinalt to the lower Late Ordovician.

Data show that the gold mineralization was emplaced during the Grampian event of the Caledonian orogeny. The ca. 10 Ma maximum possible mineralization interval (462.7–452.8 Ma) for all three episodes of gold emplacement is postpeak metamorphism and main deformation, coinciding with a period of rapid uplift and extensional tectonics following orogenic collapse. While previous studies have suggested the involvement of magmatic fluids in the deposition of the primary gold resource, the absence of magmatism throughout most of the mineralization interval and the nature of the geologic setting suggest that crustal orogenic fluids should also be considered. Overall Curraghinalt displays most of the characteristics of orogenic gold deposits but also some important differences, which may be explained by the geologic setting.

The timing of mineralization at Curraghinalt broadly coincides with the shift from compressional to extensional tectonics. The extensional regime, rapid uplift, and a crustal profile comprising metasediments overlying a still hot island arc were ideal for creating large and long-lasting hydrothermal systems deriving heat, metals, and some of the fluids from the underlying arc.

Introduction

The Curraghinalt gold deposit is hosted by quartz veins, which cut Neoproterozoic Dalradian rocks in the Sperrin Mountains, near the town of Gortin (Fig. 1). The deposit was discovered in 1983 following investigation of a soil arsenic anomaly (Earls et al., 1996) and it is now at an advanced stage of exploration. The current resource is 2.7 million ounces (Moz) Au distributed as measured: 0.02 million metric tons (Mt) @ 21.51 g/t for 10 koz, indicated: 1.11 Mt @ 12.84 g/t for 460 koz, and inferred: 5.4 Mt @ 12.74 g/t for 2.23 Moz. This makes Curraghinalt the largest known gold deposit in the British Isles.

The gold-bearing quartz veins consist of up to four generations of quartz, each deposited from a fluid of different composition and temperature (Wilkinson et al., 1999). Gold mineralization is hosted by the second and fourth generations of quartz (Earls et al., 1996; Wilkinson et al., 1999; Parnell et al., 2000). Views have changed on the genesis and timing of the first and main generations of gold mineralization. Initially it was linked to orogenic collapse during the latter part of the Grampian event of the Caledonian orogeny (Alsop and Hutton, 1993a) but later work by Hutton and others (*in* Parnell et al., 2000) linked it to late Caledonian (Siluro-Devonian) intrusive activity. The second generation of gold has been attributed to mixing of formation waters resident in Dalradian

† Corresponding author: e-mail, c.rice@abdn.ac.uk

* A supplementary Appendix to this paper is available at http://economicgeology.org/ and at http://econgeol.geoscienceworld.org/.

Submitted: May 19, 2014
Accepted: July 27, 2015

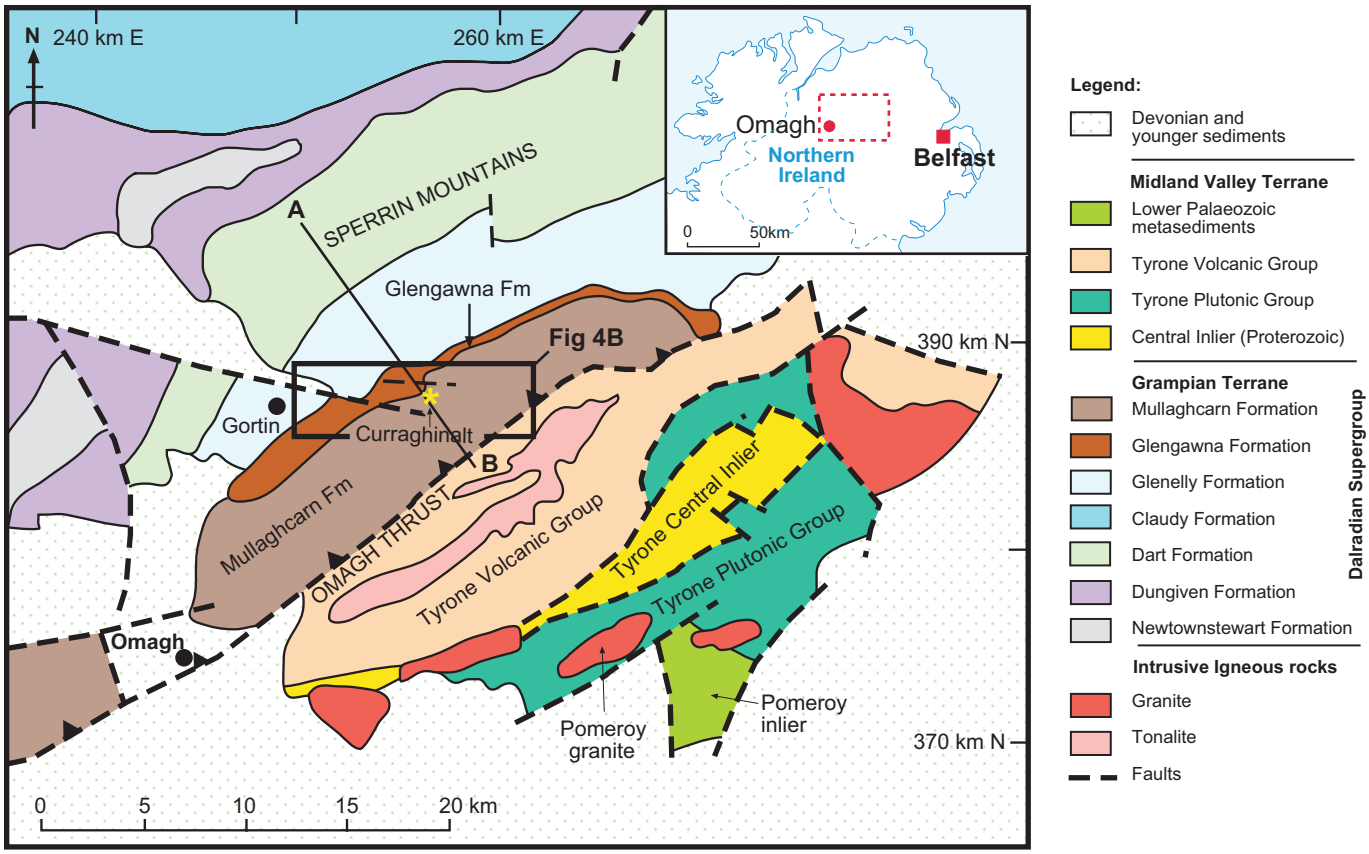

Fig. 1. Geologic map of the study area (adapted from the Geological Map of Northern Ireland, 1:250 000, GSNI, 1997). A-B marks line of section in Figure 3. Box marks area covered in Figure 4B.

metasediments with basinal brines during Carboniferous basin inversion (Wilkinson et al., 1999).

The "absolute" age of the gold mineralization, in particular, has been poorly constrained due to a paucity of critical geochronological data, which has restricted the development of a robust genetic model for Curraghinalt. A maximum age constraint is provided by the Dalradian wall rocks, which were deformed and metamorphosed during the Grampian event of the Caledonian orogeny in the period ca. 475 to 465 Ma (Dewey, 2005). Fault gouge ^{40}K-^{40}Ar ages of ca. 315 and 325 Ma from shears cutting the veins provide minimum age constraints for the gold mineralization (Earls et al., 1996; Parnell et al., 2000).

Study Aims

Despite the economic importance of quartz vein-hosted gold deposits, a number of important genetic questions remain unresolved. These include the temporal relationship between mineralization, magmatism, metamorphism, and structural events and the timing and duration of hydrothermal activity (Goldfarb et al., 2005). In this contribution we aim to address some of these outstanding issues. To do this we targeted a relatively small deposit with a large preexisting geologic and geochemical database in a well-characterized setting. Petrographic studies have been carried out on 46 polished thin sections from a representative suite of samples from seven of the ten quartz veins constituting the gold resource. This work identified sericite- and molybdenite-bearing microshears cutting the gold-bearing veins. We have dated these two minerals using the ^{40}Ar/^{39}Ar and Re-Os techniques, respectively, to provide a minimum age for the gold mineralization. Further, we have dated muscovite in wall-rock clasts contained within the veins, which offers the potential to obtain a maximum or actual age for the gold mineralization. We present a revised paragenesis and new geochronological data that show all the gold mineralization at Curraghinalt is Late Ordovician and was deposited in a relatively narrow time interval (ca. 10 Ma) during the latter part of the Grampian event of the Caledonian orogeny.

Regional Geology

The geology of the area surrounding Curraghinalt comprises three main groups of rocks: Dalradian metasediments in the Grampian terrane to the north of the Omagh thrust, the Tyrone Igneous Complex in the Midland Valley terrane to the south, and upper Paleozoic sediments which are widely distributed throughout these terranes (Fig. 1).

The Dalradian Supergroup comprises Neoproterozoic metasediments and basic metaigneous rocks deposited on the passive margin of Laurentia ca. 800 to 500 Ma (Strachan et al., 2002; Cooper and Johnston, 2004). To the southeast the NW-dipping Omagh thrust truncates the Dalradian rocks and separates them from the underlying Ordovician Tyrone Igneous Complex (Cooper and Mitchell, 2004). The Omagh thrust is part of a major terrane-bounding structure known as the Fair Head-Clew Bay Line, which is thought to be continuous with

the Highland boundary fault in Scotland. Two gold deposits, Curraghinalt and Cavanacaw, and some minor gold mineralization follow the Fair Head-Clew Bay Line in the north of Ireland. Dalradian sedimentation was terminated by an arc-continent collision in the Ordovician (Grampian event of the Caledonian orogeny; Hollis et al., 2013a). Polyphase deformation and regional metamorphism in the Dalradian of western Ireland is dated to between ca. 475 to 465 Ma (Friedrich et al., 1999).

There are three main lithologic groups in the rocks to the south of the Omagh thrust, the Tyrone Central Inlier, the Tyrone Plutonic Group, and the Tyrone Volcanic Group (Fig. 1). The last two constitute the Tyrone Igneous Complex (Cooper and Mitchell 2004). The Tyrone Central inlier is composed of psammitic and semipelitic paragneisses, known as the Corvanaghan Formation (Cooper and Johnston, 2004) that are closely associated with syntectonic leucosomes (U-Pb, ca. 467 Ma, Chew et al., 2008) and are cut by post-tectonic pegmatites. Biotite cooling ages imply that the Tyrone Central inlier was metamorphosed and deformed prior to ca. 468 Ma (Chew et al., 2008). Detrital zircon age profiling suggests an upper Dalradian Supergroup affinity for the Tyrone Central inlier and as such it is interpreted to represent part of an outboard segment of Laurentia, possibly detached as a microcontinent prior to arc continental collision (Chew et al., 2008). The Tyrone Plutonic Group represents the uppermost portion of a ca. 484 to 480 Ma suprasubduction zone ophiolite accreted with the ca. 475 to 469 Ma Tyrone Volcanic Group island arc onto an outboard microcontinental block prior to ca. 470 Ma during the Grampian event of the Caledonian orogeny (Cooper et al., 2008, 2011; Hollis et al., 2012, 2013a, b). Various arc-related granitoids intruded the Tyrone Volcanic Group following a reversal of subduction polarity and have been dated at ca. 470 to 464 Ma (Cooper et al., 2011).

The Grampian orogeny resulted in crustal thickening, nappe structures, and metamorphism (Cooper and Johnston, 2004). Collapse of the orogenic pile followed during the interval ca. 470 to 450 Ma, accompanied by exhumation, extension, and partial melting (Alsop and Hutton, 1993a; Flowerdew et al., 2000; Clift et al., 2004). Final closure of the Iapetus Ocean occurred during the mid-Silurian and resulted in another orogenic event, the Scandian event of the Caledonian orogeny, marked in the north of Ireland by magmatism and further deformation and metamorphism (Kirkland et al., 2013).

Curraghinalt: Geology and Mineralization

In detail the country rocks hosting the gold veins mirror the regional deformation picture (Fig. 2). The dominant structure is the Sperrin nappe and the veins lie on the inverted, NW-dipping limb of this fold (Alsop and Hutton, 1993b; Fig. 3). Peak metamorphism to upper greenschist facies was reached during D_3, which is the final compressional phase of the Grampian event. D_3 in the Sperrin Mountains marked the emplacement from the northwest of the Dalradian Supergroup over the Tyrone Igneous Complex and Tyrone Central inlier along the Omagh thrust. This event appears to overlap with the intrusion of a suite of arc-related plutons into the Tyrone Volcanic Group between ca. 470 to 464 Ma (Cooper et al., 2008, 2011; Hollis et al., 2012, 2013b), the youngest of which is dated to ca. 464 Ma. This provides a maximum age constraint of ca. 464 Ma for the gold mineralization at Curraghinalt since the quartz veins were not affected by D_3. D_3 was followed closely by regional-scale extensional shearing attributed to orogenic collapse and in the Sperrin Mountains, this was accompanied by NE-trending quartz veins (Alsop and Hutton, 1993a).

The reported gold resource is distributed within a swarm of 10 NW-SE-oriented and steeply NE dipping quartz veins that are mainly hosted by semipelites of the Dalradian Argyll Group

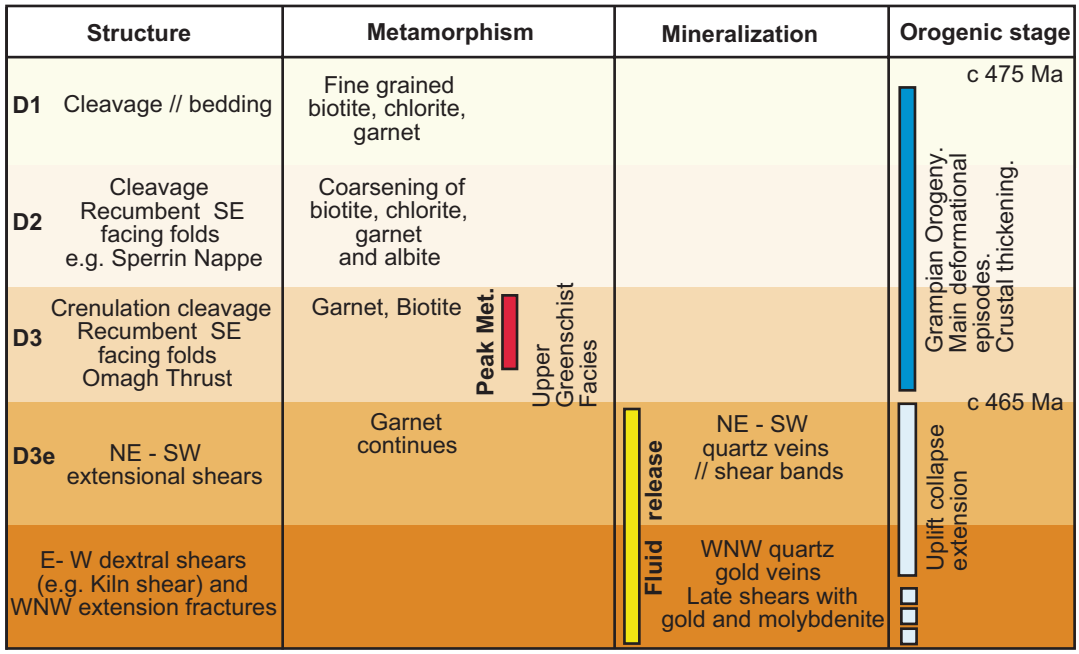

Fig. 2. The Grampian event in the Sperrin Mountains: Summary of structure, metamorphism, and mineralization (adapted from Alsop and Hutton, 1993a, b; Parnell et al., 2000; and present study).

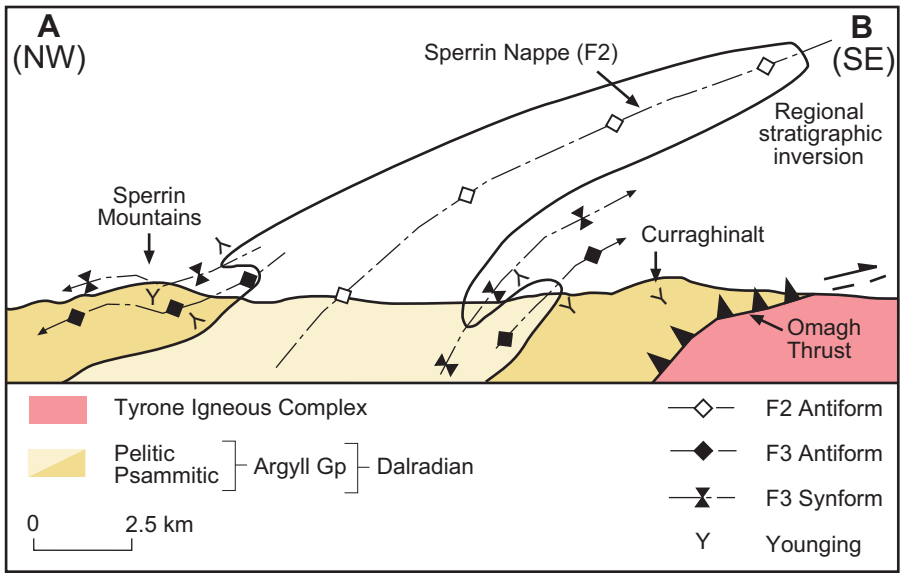

Fig. 3. Section across the Sperrin nappe and Omagh thrust and location of the Curraghinalt gold deposit (simplified after Alsop and Hutton, 1993b; line of section in Fig.1). Note that there is a difference of opinion on the position of the axis of the Sperrin nappe between GSNI (Fig. 1) and Alsop and Hutton (1993b).

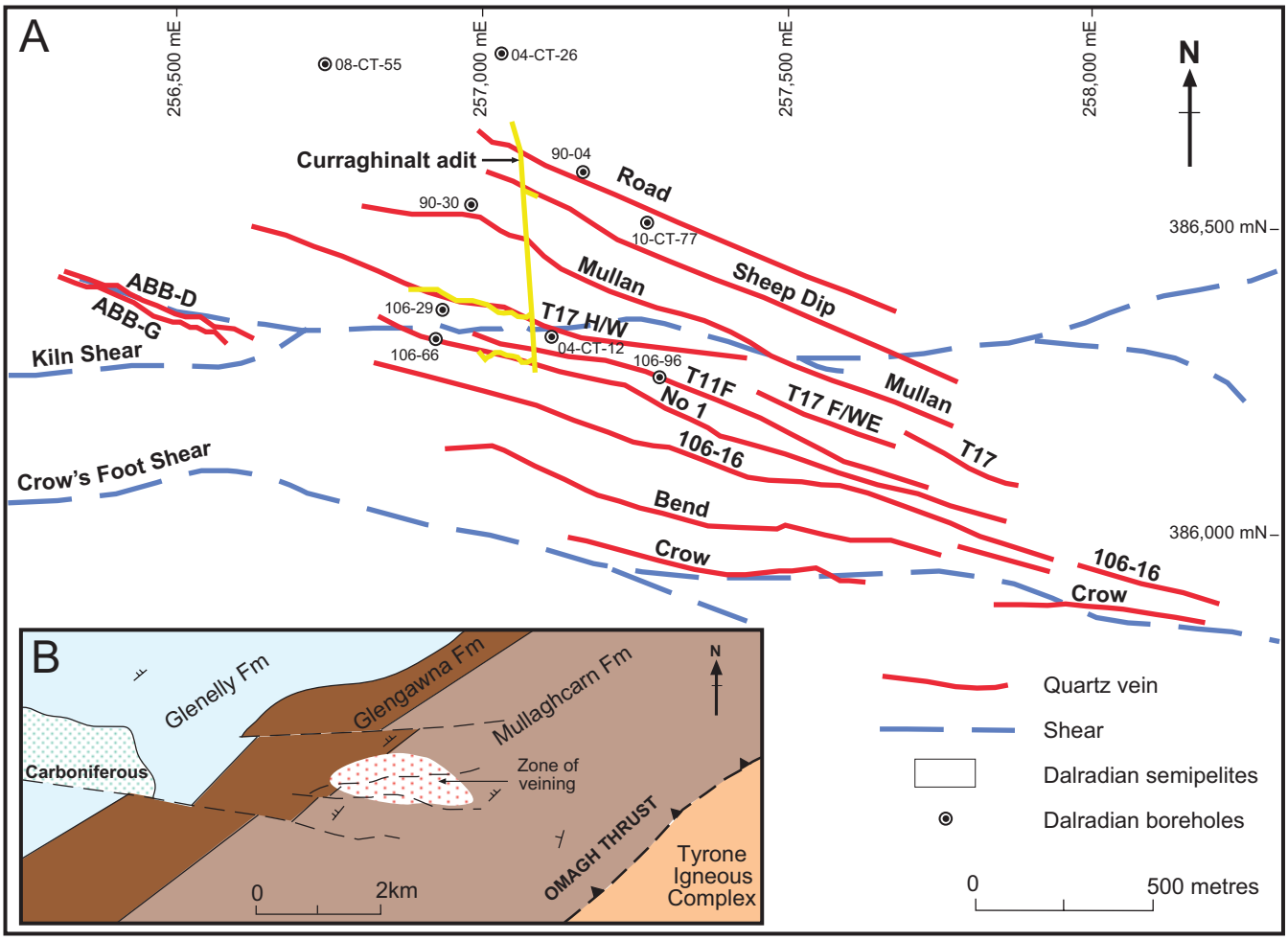

Fig. 4. (A). Deposit geology showing the 10 veins hosting the gold resource, the Kiln and Crows Foot shears, and the adit (courtesy Dalradian Gold Ltd.). (B). Local geology of the Curraghinalt gold deposit (area covered shown in Fig. 1).

(Fig. 4A). The limits of the veins are mainly defined by drilling and their full extent along strike and downdip is unknown. The resource is close to the contact between the Glengawna (graphitic pelites, semipelites, and psammites) and Mullaghcarn (psammites and semipelites) Formations (Earls et al., 1996; Lawther and Moloney, 2012; Fig. 4B). Two generations of gold mineralization have been identified (Wilkinson et al., 1999; Parnell et al., 2000). The first generation (Q2) is the most economically important and this gold contains small quantities of silver and is accompanied by arsenopyrite, tellurides, and most of the pyrite, whereas the second (Q4) contains more silver and is accompanied by most of the Sb-As sulfosalts, chalcopyrite, and barite and all of the carbonates (Fig. 5A).

Two major E-W-trending and steeply dipping shear zones cut the veins: the Kiln and Crows Foot shears (Fig. 4A). These are part of a 1-km-wide belt of faults that can be traced for several kilometers (Fig 4B). They are aligned with a reentrant in the Omagh thrust zone and are consistent with a lateral ramp in the footwall of the thrust (Parnell et al., 2000). Some of the veins and the Kiln shear are exposed in an adit driven to investigate the Curraghinalt mineralization below surface (Fig. 4A). Dextral movement on the shears is thought to be responsible for the formation of the vein-hosting structures (Clifford et al., 1992; McCaffrey and Johnston, 1996).

A major structural control on the vein-filling structures has been attributed to repeated movements of the Omagh thrust over the footwall ramp. Thus, Parnell et al. (2000) proposed episodic E-SE-directed thrusting of the Dalradian over the Tyrone Igneous Complex over a prolonged period of time (Ordovician to Carboniferous), which led to reactivation of structures hosting the veins and emplacement of the different generations of mineralization. It was suggested that the main (first) generation of gold mineralization was related to Late Caledonian (Siluro-Devonian) movements. In contrast, Alsop and Hutton (1993a) proposed that the gold mineralization (undifferentiated) was related to fluid release during NW-directed downdip extension in the hanging wall of the Omagh thrust. This was linked to collapse of the Sperrin nappe in the latter stages of the Grampian event of the Caledonian orogeny.

The veins are cut by NE-trending, NW-dipping normal faults (Parnell et al., 2000), which may be linked to further collapse of the Sperrin nappe, or a later unrelated extensional episode.

Petrographic Study of the Sericite- and Molybdenite-Bearing Microshears

Field relationships

The microshears have been observed in situ in the Curraghinalt adit only, where they cut the T17 vein (Figs. 4A, 6). Here the shears are thin (ca. 1 mm) and dark gray. They are subvertical and strike roughly east-west and as such they are essentially parallel to the Kiln shear, which cuts the T17 vein at this point. Whether this is due to rotation of the T17 vein within the Kiln shear zone (G. Earls, pers. commun.) or is a primary orientation remains unknown. Their orientation in core and the deposit-wide orientation is also currently unknown.

The microshears have been identified in six out of seven quartz veins sampled and in 22 out of the 46 polished thin sections we examined. It is uncertain whether the shears are restricted to veins. While they can be readily identified megascopically in quartz veins, they are difficult to see in pelitic wall rock. However, the presence of numerous Mo-rich zones in wall-rock intersections in cores suggests that they are present.

Mineralogy

The microshears range in thickness from 0.05 to 1 mm and consist predominantly of fine-grained (10–30 μm) sericite with patchy and locally abundant molybdenite, minor pyrite, and rare carbonate, chalcopyrite, electrum (at. % Au 65.0–78.9), a Bi-Ag telluride, a Ti oxide, zircon, and apatite (Fig. 7). Quartz adjacent to the sericite may be locally fine grained and recrystallized, reflecting granulation during brittle shearing. There are some mineralogical similarities between the microshears and the two stages of sulfide and precious metal mineralization recognized by Parnell et al. (2000), such as pyrite, chalcopyrite, a Bi telluride, and electrum. However, there are

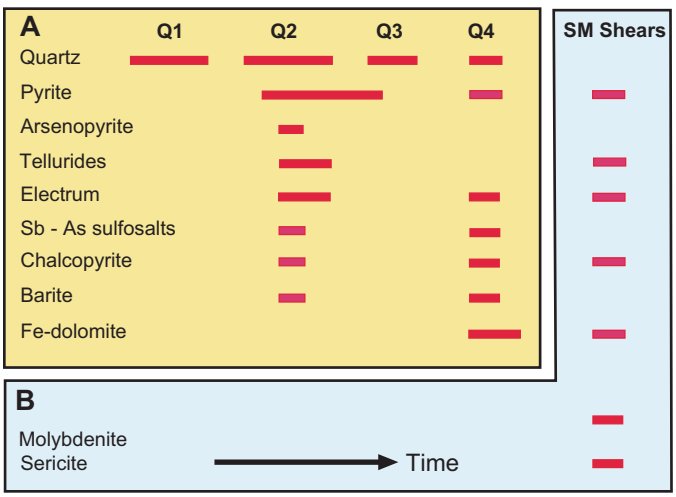

Fig. 5. (A). Paragenesis of the Curraghinalt gold deposit after Parnell et al. (2000). (B). Addition to paragenesis from present study.

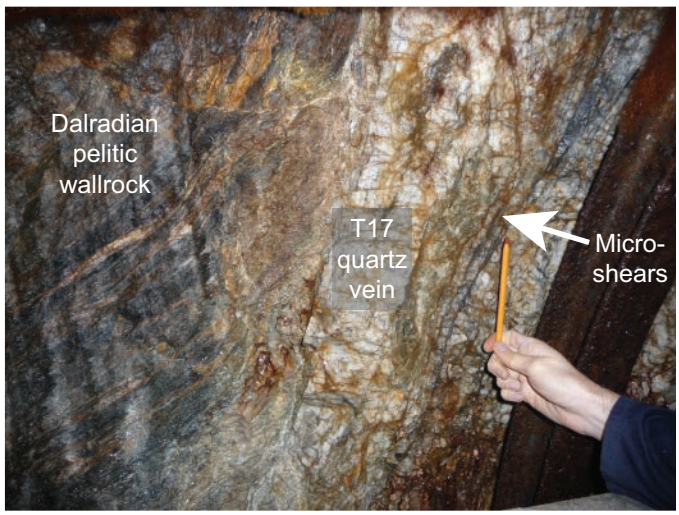

Fig. 6. Curraghinalt adit. T17 vein cutting the dominant S_2/S_3 regional foliation in pelitic wall rock. Subvertical dark microshears showing a horsetail splay structure can be seen in the vein (tip of pen).

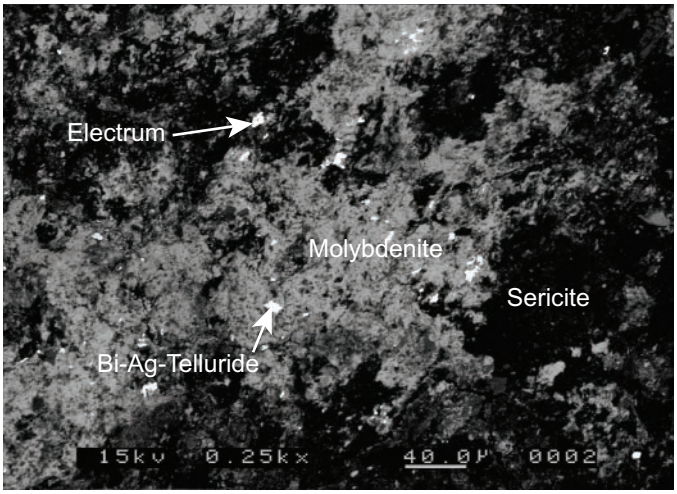

Fig. 7. BSEM image of microshear (Sheep Dip vein, sample B1633), showing sericite (dark gray), molybdenite (light gray), Bi-Ag telluride, and electrum.

also important differences (i.e., the presence of molybdenite and sericite and the absence of quartz).

Paragenesis

A detailed study of the 45 polished thin sections (Table 1A) provided by Dalradian Gold plus 1 polished thin section (A3929) selected by ourselves, using combinations of transmitted light (TL), reflected light (RL), backscanning electron microscopy (BSEM), and cathodoluminescence (CL), was carried out to characterize and establish precisely the paragenetic position of the microshears. During the course of this work the deposit paragenesis of Earls et al. (1996) and Parnell et al. (2000) was confirmed. Some of the BSEM and the entire quantitative mineral analyses were carried out in the Department of Geology and Petroleum Geology, University of Aberdeen, using an ISI-ABT55 SEM fitted with a LINK ANALYTICAL AN10/55S system. Quantitative analyses were acquired and processed with the LINK ZAF4/FLS program. The combined BSEM and CL studies were carried out at the Imaging Spectroscopy and Analysis Centre (ISAAC) facility of the University of Glasgow with an FEI Quanta 200F field emission SEM using a KE developments panchromatic CL detector.

Table 1a. Locations for Samples Examined Using BSEM-CL (vein and borehole locations in Fig. 4)

Sample no.	Vein	Borehole ID	From (m)	To (m)
A3929	1	08-CT-55	426	426.15
DAL 25	106-16	106-96	124.64	126.21
DAL 27	106-16	106-66	87.20	88.37
DAL 33	106-16	106-29	127.84	129.42

[1] Unnamed quartz vein in zone between the T17 and 1 veins

Table 1b. List of Samples Used in the Main Petrographic Study (vein and borehole locations in Fig. 4)

Vein	Sample no.
106.16	DAL 22, 23, 24, 25, 26, 27, 33, 48
T17C	DAL 7, 9, 10, 11, 39, 50
T11F	DAL 14, 15, 16, 28, 37, 49
No 1	DAL 17, 18, 19, 20, 21, 30, 32, 51, 52
ABB	DAL 34, 45, 46
T17HW	DAL 1, 3A, 3B, 4, 5, 6, 53, 54, 55
Sheep Dip	DAL 41, 42, 43

An important feature of the earlier studies by Wilkinson et al. (1999) and Parnell et al. (2000) is that, using combined CL and BSEM analysis, four generations of quartz (Q1-Q4) were recognized within the deposit. Two of these (Q2 and Q4) have been linked to episodes of gold sulfide mineralization (Wilkinson et al., 1999, Parnell et al., 2000). Our combined CL/BSEM analysis focused on four polished thin sections from a main vein (106.16) and an unnamed minor vein (Table 1B), which showed critical relationships between the microshears and key minerals in the deposit paragenesis.

All four sections showed four generations of quartz generally similar in character to those described by Wilkinson et al. (1999) and Parnell et al. (2000; Fig. 8A, B). In all sections Q1 and Q2 are volumetrically the most important. These two generations of quartz show some differences from these earlier studies in terms of the clast to cement ratio and the presence of zoning. While Q1 is only seen as clasts, as reported by Wilkinson et al. (1999) and Parnell et al. (2000), the proportion of Q2 cement varies significantly, so that some breccias are clast supported and may contain minimal amounts of "dark" (in CL) Q2 cement, whereas others are more fully cemented and Q2 may be the dominant component. Also, Q1 clasts showing oscillatory zoning are common and some sector zoning may be present (Fig. 8A, B). Q3 occurs in veinlets cutting Q1 clasts and Q2 cement. Under CL imaging, it can show concentric zonation but does not have the brecciated appearance of Q1 (Fig. 8A). The final generation of quartz (Q4) shows the brightest luminescence of all and cuts all previous generations of quartz and early pyrite (Fig. 8A).

Various crosscutting relationships show that the microshears not only postdate gold-bearing pyrite of the first generation of gold mineralization (Q2) but importantly, also quartz, chalcopyrite, and carbonates of the second generation of gold mineralization (Q4) (Figs. 9, 11–13). Second generation chalcopyrite was distinguished on the basis of contained angular inclusions of arsenopyrite (Fig. 10) (unique to stage 1 mineralization, Parnell et al., 2000) and also inclusions of electrum with at. % Au in the range 69.2 to 77.9 (characteristic of second generation gold, Parnell et al., 2000). Fe-rich carbonates are characteristic of the second generation of gold mineralization and continued crystallizing after the other minerals (Parnell et al., 2000, fig. 8). We have observed carbonates (siderite) not only being cut by the microshears (Fig. 13A) but also rare ferroan dolomite veins cutting the microshears (Fig. 13B). No sulfide-bearing veins have been observed cutting the microshears.

These relationships show clearly that the microshears are a new third generation of sulfide and gold mineralization and, accordingly, we present a revised paragenesis (Fig. 5A, B). Thus, by dating the microshears, a minimum age for the first two generations of gold mineralization can be obtained.

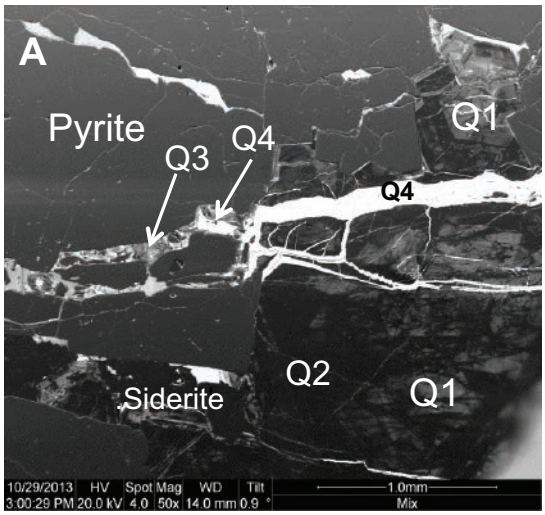

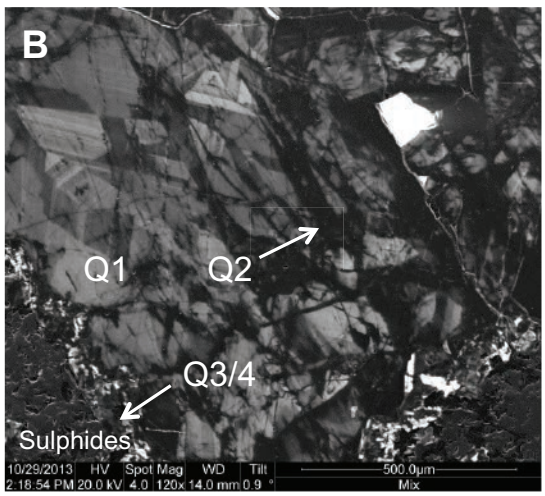

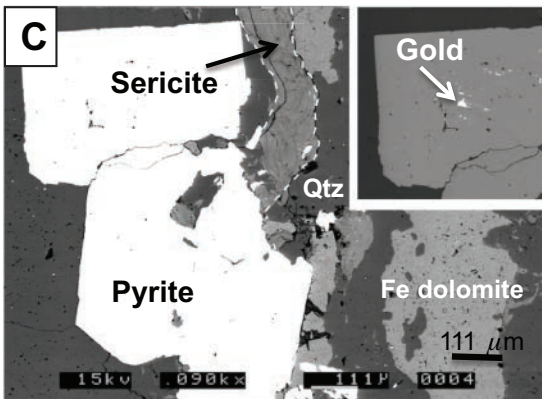

Fig. 8. (A). BSEM/CL image (unnamed quartz vein in zone between T17 and 1 veins; sample A3929, loc. Table 1 and Fig. 9). Q1 clasts showing concentric zoning, cemented by dark Q2. Q1, Q2, and early pyrite are cut by veinlets of Q3 showing concentric zoning. Bright Q4 cuts Q3. Q3 and Q4 appear to replace siderite. (B). BSEM/CL image (same sample as Fig. 8A). Q1 clasts showing concentric and sector zoning and cemented by dark Q2. Q3 and Q4 occur along the contact between Q1/Q2 and sulfides. (C). BSEM image (106-16 vein, sample DAL 25). Sericite in microshear cutting early pyrite (arrowed) with gold inclusions (inset). These pyrites contain rounded gold inclusions away from edges and fractures with at. % Au 93-94 interpreted as first generation gold and gold associated with fractures with at. % Au 83-84 interpreted as second or third generation gold (associated with the microshears).

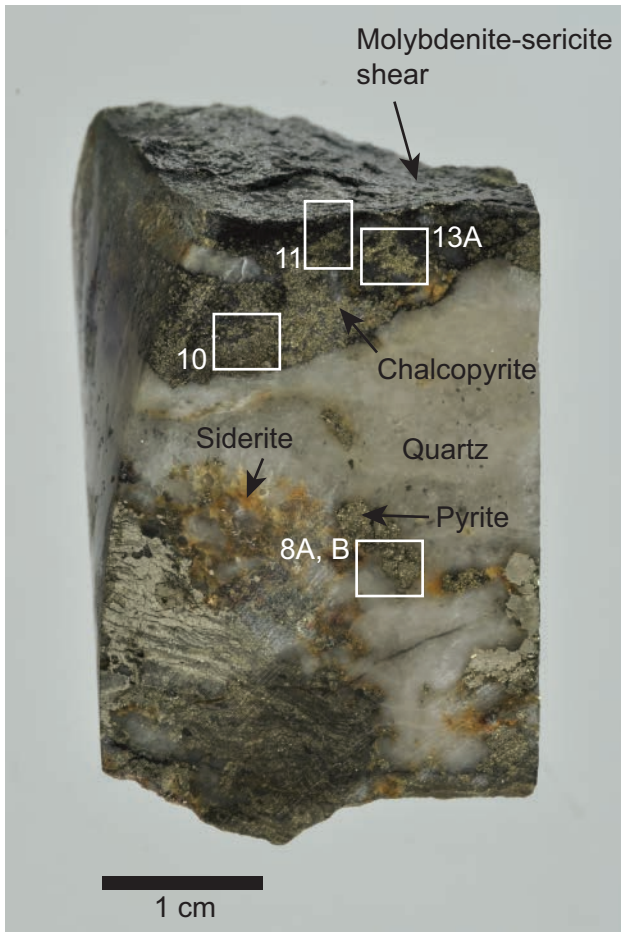

Fig. 9. Core sample A3929, loc. Table 1). Sericite- and molybdenite-bearing microshear cutting chalcopyrite of the second generation of gold mineralization. Also visible are first generation pyrite and second generation siderite. Boxes show locations of Figures 8A, B, 10, 11, and 13A.

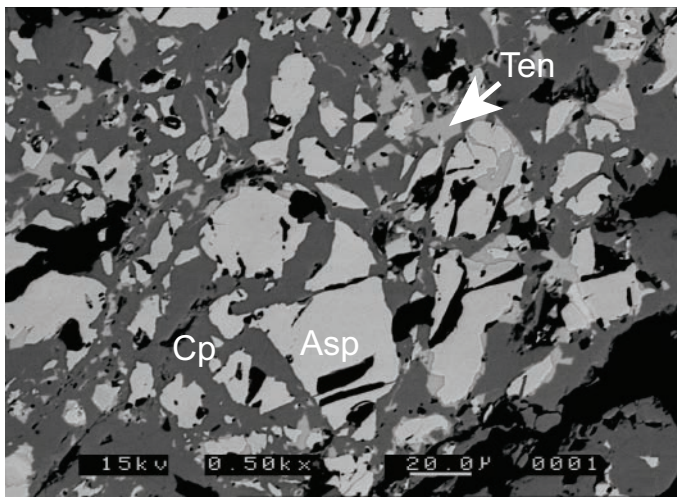

Fig. 10. BSEM image (sample A3929, loc. Table 1, Fig. 9). Chalcopyrite (cp) and tennantite (ten) (second generation of gold mineralization), cementing angular fragments of arsenopyrite (asp) (first generation of gold mineralization).

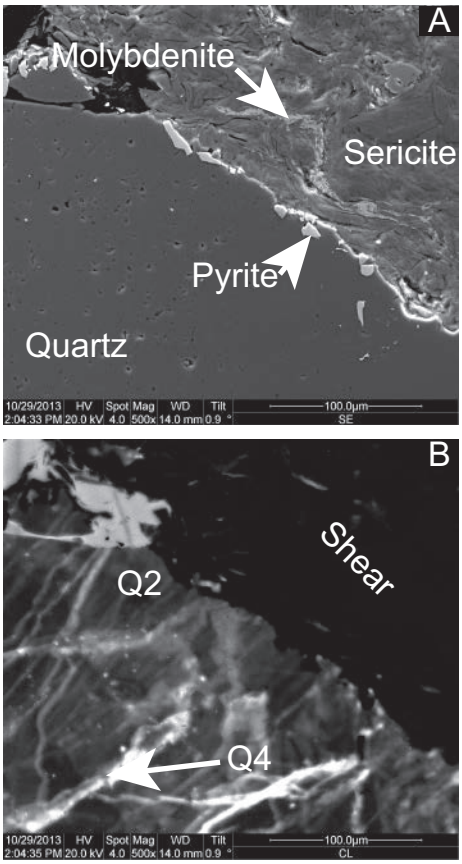

Fig. 11. (A). (BSEM image; sample A3929, loc. Table 1, Fig. 9). Microshear composed of mainly sericite with minor molybdenite cutting quartz vein. Sheared pyrite occurs along the contact. (B). Same view as (A). CL image of the microshear cutting veinlets of Q3 and Q4 (brightest) hosted by dark Q2. Light patch at top left is a hole in the slide.

Dating the Gold Mineralization

During the petrographic study we searched for minerals with which to directly date the gold mineralization. The only possibilities found were pyrite and chalcopyrite but their Re contents were too low (<0.5 ppb) for determination of precise Re-Os ages. As a result we decided to date metamorphic muscovite in wall-rock clasts enclosed within the quartz veins in the hope that the $^{40}Ar/^{39}Ar$ systematics of the muscovite had been reset by the thermal pulse associated with the first generation of gold (below). Constraints on the maximum age of mineralization are already provided by the age of regional metamorphism, and deformation of the vein wall rocks, and by a D_3 deformed granite located within the Tyrone Igneous Complex (ca. 464 Ma, discussed above). Dating of the sericite-molybdenite shears (third gold phase) would provide a minimum age for the first and second generations of gold mineralization (the main resource). This approach will allow for temporal constraints to be placed on the duration of mineralization.

Estimate of maximum age of mineralization

The gold-bearing quartz veins contain clasts of pelitic wall rock (Figs. 14, 15) as well as of quartz (Q1). The pelitic clasts are largely composed of muscovite that shows a strong foliation,

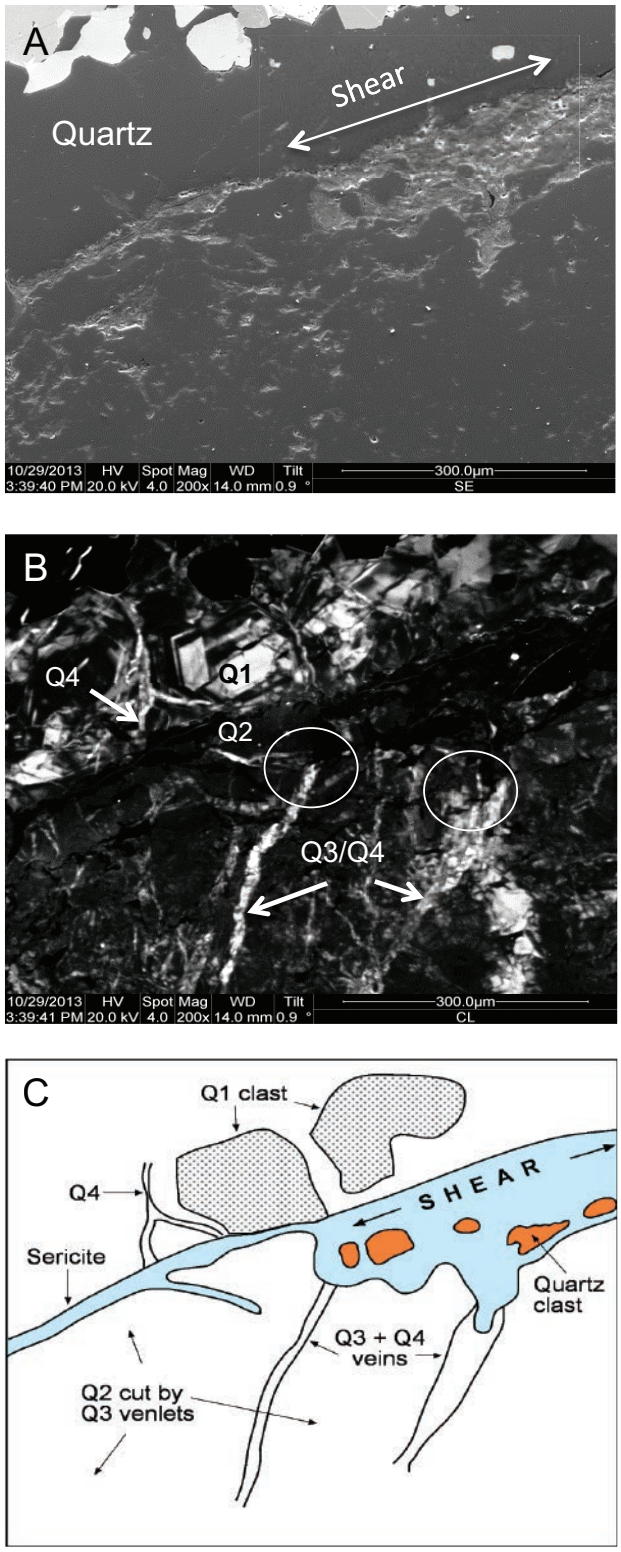

Fig. 12. (A). BSEM image (vein 106.16, sample DAL 27). Microshear composed of sericite (light gray) with clasts of quartz cutting vein quartz (see schematic Fig. 12C). (B). CL image. Circled areas show mixed veinlets of Q3 and Q4 truncated by irregular shear surface. Adjacent to mixed veinlets are numerous Q3 veins cutting dark Q2. Fine Q4 veinlets, also truncated, can be seen on the opposite side of the shear. Movement along the shear is demonstrated by nonmatching quartz stratigraphy in the opposing wall rock (see schematic in C).

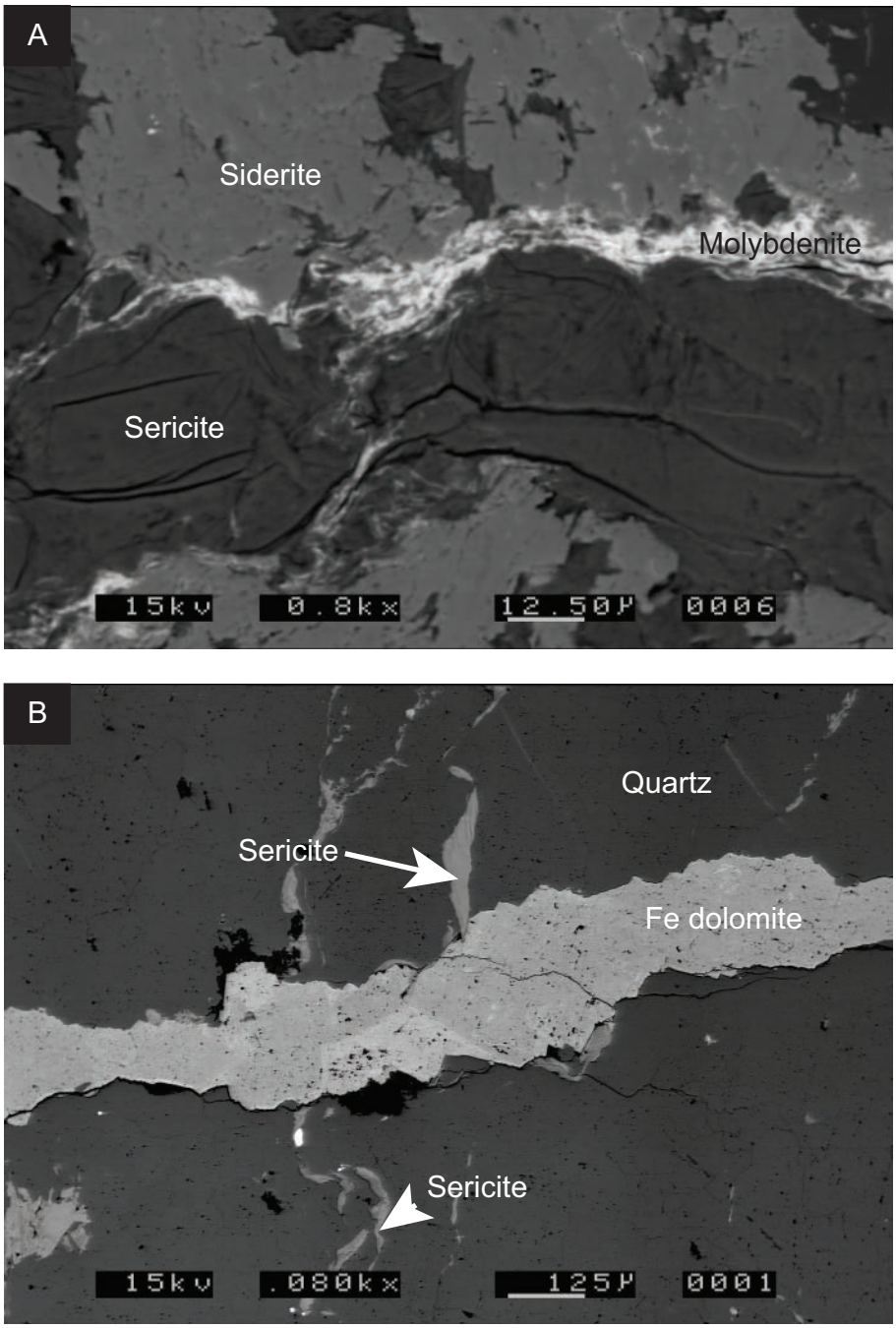

Fig. 13. (A). BSEM image (sample A3929, Table 1, Fig. 9). Sericite- and molybdenite-bearing microshear cutting siderite (second generation of gold mineralization). (B). BSEM image (vein 106.16, sample DAL 25). Ferroan dolomite-filled fracture cutting sericite-bearing microshear.

probably corresponding to a composite S_2-S_3 fabric developed over much of the Sperrin Mountains (Alsop and Hutton, 1993a). Minerals from the first two generations of gold mineralization fill the spaces between different clasts within the veins and thus demonstrate that clast formation predated these mineralization events. Providing there has been no thermal disturbance to the muscovite $^{40}Ar/^{39}Ar$ systematics then an $^{40}Ar/^{39}Ar$ age would provide a maximum age for gold mineralization, the muscovite $^{40}Ar/^{39}Ar$ age potentially recording the time at which the terrane cooled from peak metamorphic temperatures (ca. 475–465 Ma, discussed above) through the muscovite closure temperature (T_c) window (ca. 400°C). However, we know that the maximum ambient fluid temperature (T_{max}) reached during the first generation of gold mineralization was ca. 400°C (Parnell et al., 2000) and as such, we have to consider the possibility that the $^{40}Ar/^{39}Ar$ system will have been reset and potentially that the muscovite may record the actual age of this generation of mineralization

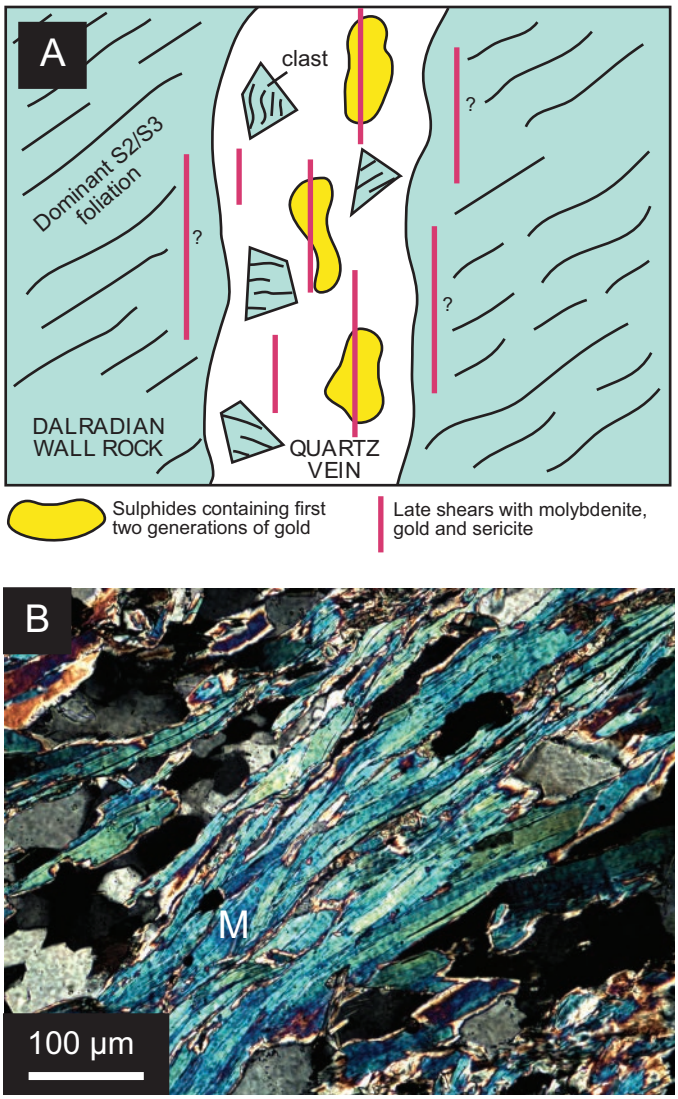

Fig. 14. (A). Cartoon showing the paragenetic relationships of the dated samples. (B). Metamorphic muscovite (M) in semipelite clast from dated sample DAL 49 (Table 2, Fig. 15E).

(i.e., the $^{40}Ar/^{39}Ar$ system will postdate the age at which the terrane cooled through the muscovite closure temperature). The degree of resetting will be dependent on the duration of T_{max} as well as the effective diffusion dimension (i.e., crystal radius) of the muscovite Ar diffusion domain (e.g., Mark et al., 2008; Harrison et al., 2009). Note that the maximum fluid temperatures of the second stage of gold mineralization are significantly below the muscovite closure temperature and thus later resetting of the system is unlikely.

Estimate of minimum age of mineralization

Dating of sericite and molybdenite in the sericite-molybdenite shears that cut Q1-Q4 will not only provide a direct age for the newly discovered third generation of gold mineralization, but will also constrain a minimum age for the first two generations of gold mineralization. Note that shearing is a mechanical process and on the scale observed within the polished thin sections this process will have had no impact on the $^{40}Ar/^{39}Ar$ systematics of the muscovite within the wall-rock clasts (Kirkpatrick et al., 2012).

Samples for radioisotopic dating

All samples for dating (Re-Os and $^{40}Ar/^{39}Ar$) were obtained from core and hence have good geologic context as well as petrographical control. Sericite-molydenite shears were located during the petrographic study and also by examining Mo-rich intersections identified from assay data. The majority of the shears found by the latter method lacked sufficient molybdenite for Re-Os dating, although most had sufficient sericite for $^{40}Ar/^{39}Ar$ dating. Only one sample (B1633) had sufficient quantities of both minerals for a dual analysis using both techniques. Suitable wall-rock clasts within quartz veins were identified during the petrographic study and sections/wafers of rock were prepared for dating. The four shears selected for dating are from two of the main veins (Sheep Dip and 106-16) and have similar characteristics (grain size, thickness, mineralogy) to those seen in all the examined samples (Table 2). Specifically, we dated a shear with coexisting sericite and molybdenite and a shear containing sericite only from the Sheep Dip vein, and molybdenite and sericite from separate shears cutting vein (106-16).

Muscovite within three wall-rock clasts hosted by two different gold-bearing veins (DAL 49 and DAL 6) were targeted for in situ UVLAMP (e.g., Mark et al., 2010b) $^{40}Ar/^{39}Ar$ dating (Fig. 15). The clasts are muscovite rich and show a foliation typical of the pelitic wall rocks (Fig. 14B). The muscovites show no trace of alteration or recrystallization.

Two samples of molybdenite-bearing shears (A8406 and B1633) were selected for Re-Os analysis (Fig. 7, Table 2). Two sericite-bearing shears were also targeted for in situ UVLAMP

Table 2. Sample Locations and Identifiers, Targeted Mineral Phases for Radioisotopic Dating and Geochronological Methods/Techniques Applied

Sample no.	Vein	Borehole ID	From (m)	To (m)	Target mineral	Location	Number analyzed	Method	Technique
DAL 42	Sheep Dip	90-04	66.26	66.45	Sericite	Shear	1	$^{40}Ar/^{39}Ar$	UVLAMP
DAL 33	106-16	106-29	127.84	129.42	Sericite	Shear	3	$^{40}Ar/^{39}Ar$	UVLAMP
B1633	Sheep Dip	04-CT-26	182.00	182.25	Sericite[1]	Shear	1	$^{40}Ar/^{39}Ar$	Step Heating
					Molybdenite[1]	Shear		Re-Os	ID-NTIMS
A8406	106-16	10-CT-77	310.22	310.35	Molybdenite	Shear	1	Re-Os	ID-NTIMS
DAL 49	T11F	04-CT-12	60.09	61.42	Muscovite	Clast	1	$^{40}Ar/^{39}Ar$	UVLAMP
DAL 6	T17HW	90-30	164.27	165.48	Muscovite	Clast	2	$^{40}Ar/^{39}Ar$	UVLAMP

Notes: Abbreviations: ID-NTIMS = Isotope dilution negative ion thermal mass spectrometry; UVLAMP = UV laser ablation microprobe
[1] Molybdenite and sericite coexisting on the same shear

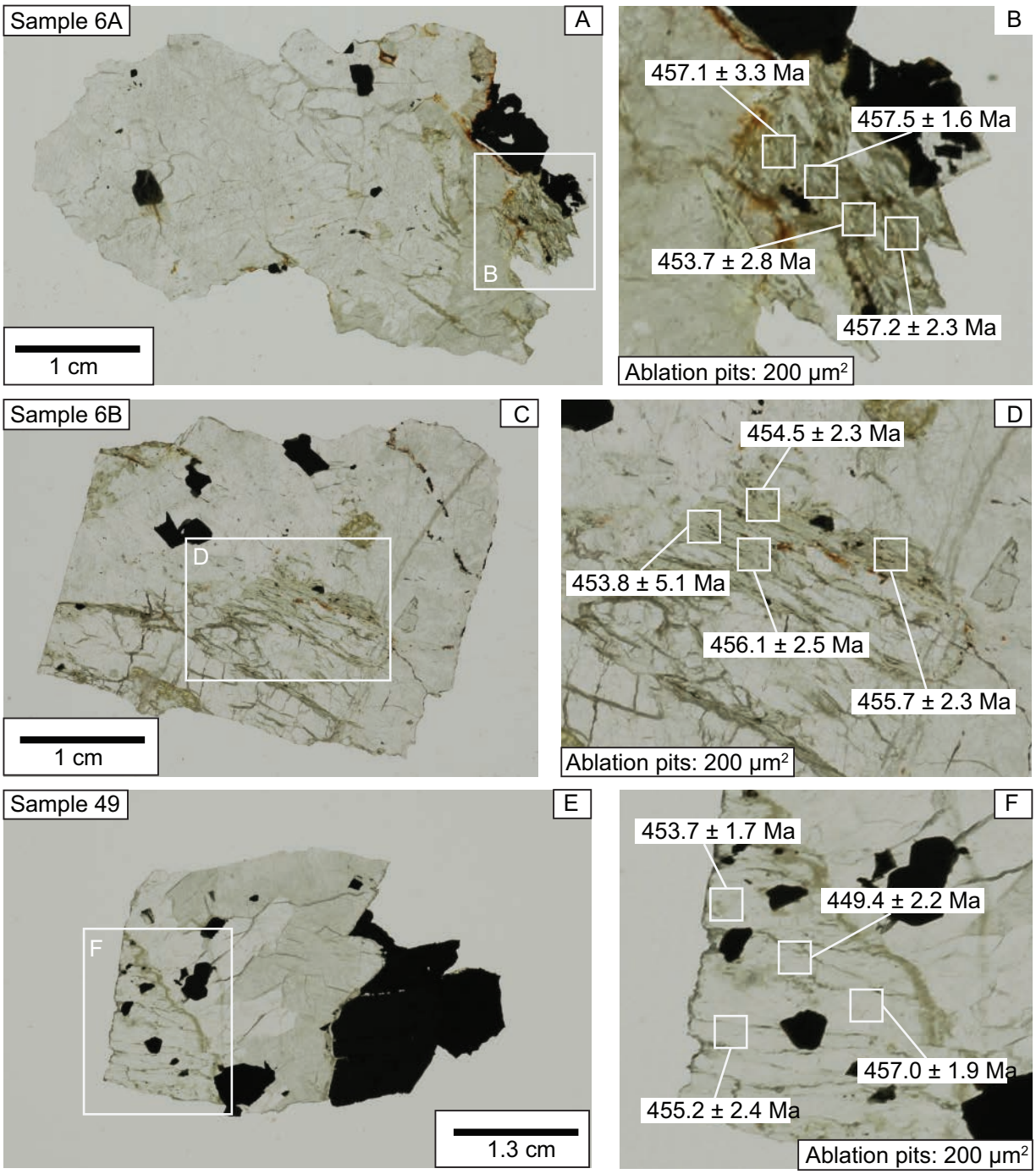

Fig. 15. $^{40}Ar/^{39}Ar$ age data for muscovite from within quartz vein-hosted wall-rock clasts. Photomicrographs showing in situ UVLAMP $^{40}Ar/^{39}Ar$ age data within a petrographical context. All $^{40}Ar/^{39}Ar$ age data reported at 1σ (analytical precision) using the decay constants of Steiger and Jaeger (1977) and the standard ages of Renne et al. (1998).

(e.g., Mark et al., 2007) $^{40}Ar/^{39}Ar$ dating within two different gold-bearing veins (DAL 33 and DAL 42; (Fig. 16, Table 2). A third fine-grained sericite- and molybdenite-bearing shear from a different vein (B1633, Fig. 7) was also analyzed. The sericite in this sample was sufficiently abundant for harvesting using standard mineral preparation techniques (e.g., Mark et al., 2010a) and subsequent $^{40}Ar/^{39}Ar$ incremental step-heating (e.g., Mark et al., 2011a).

Analytical Methods

Re-Os dating

Two molybdenite separates from sample A8406 were obtained. One separate was isolated using traditional mineral separation protocols, e.g., crushing, magnetic Frantz separation, heavy liquids, and water flotation (Selby and Creaser, 2004). Although several tens of milligrams were isolated the

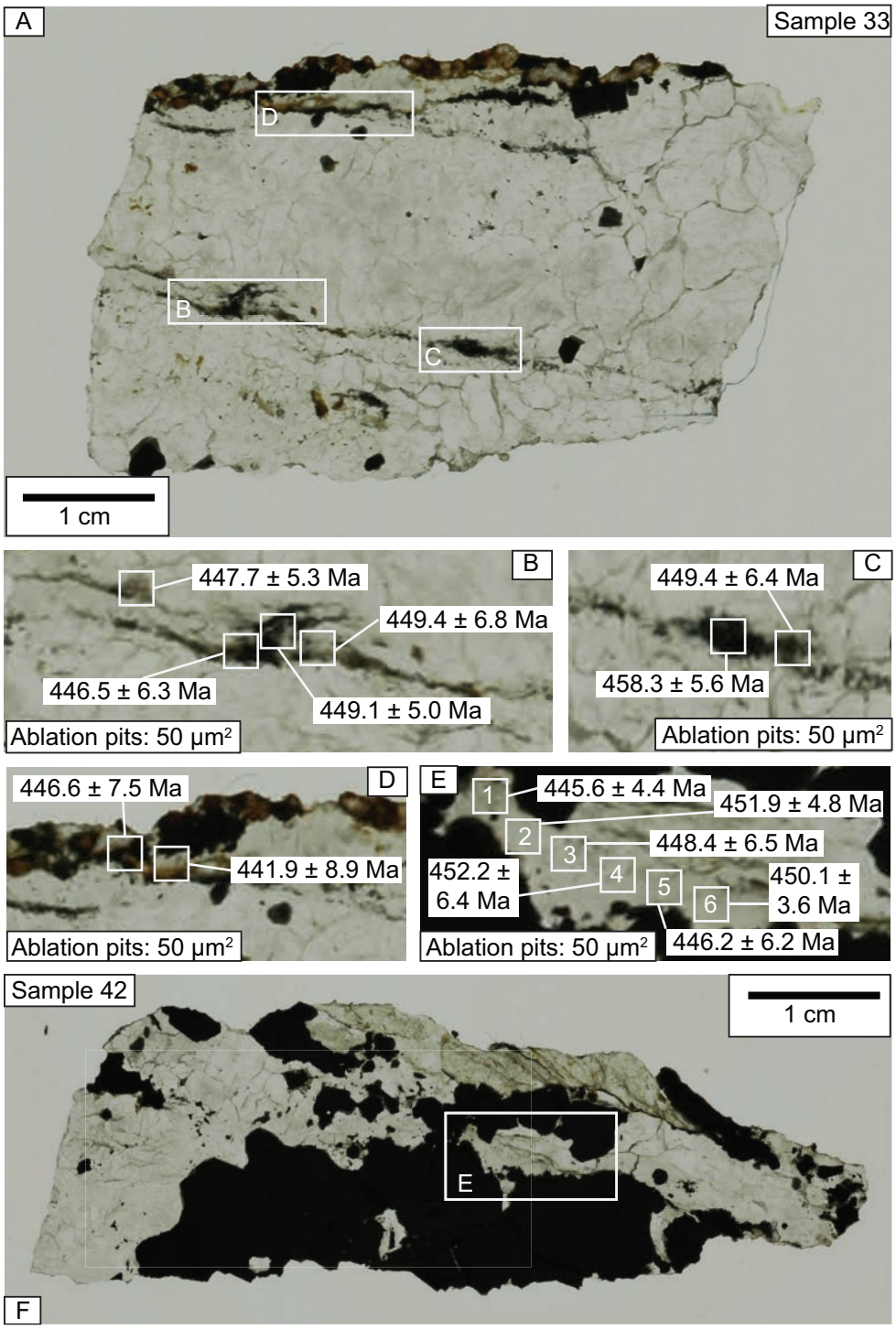

Fig. 16. $^{40}Ar/^{39}Ar$ data for sericite in microshears hosted by quartz veins. Photomicrographs showing in situ UVLAMP $^{40}Ar/^{39}Ar$ age data within a petrographical context. All $^{40}Ar/^{39}Ar$ age data reported at 1σ (analytical precision) using the decay constants of Steiger and Jaeger (1977) and the standard ages of Renne et al. (1998).

molybdenite in sample A8406 was extremely fine grained and thus much of the molybdenite remained either enclosed in the quartz vein or was lost in the fine fraction during sieving or washing of the sample. A second mineral separate was achieved utilizing the HF isolation approach (Lawley and Selby, 2012). The latter uses concentrated HF at room temperature for the digestion of the silicate material hosting the molybdenite. Molybdenite from sample B1633 was also isolated using the HF method.

The Re-Os analytical protocol follows that described by Selby and Creaser (2001), with a slight modification to the isolation protocol of Re. An aliquot of molybdenite doped with a

known amount of tracer solution comprising ^{185}Re and normal Os isotope composition was loaded into a carius tube with a 1/3 mL mix of concentrated HCl and HNO_3 and sealed, and then heated to 220°C for 24 hours Os was isolated from the acid solution using solvent extraction with $CHCl_3$ and further purified using microdistillation. The Re was isolated using solvent extraction by NaOH and Acetone, and then further purified using anion HNO_3/HCl chromatography. The Re and Os fractions were analyzed for their isotope compositions using negative Thermal ionization mass spectrometry (N-TIMS, Creaser et al., 1991; Volkening et al., 1991) using a Thermo Electron TRITON mass spectrometer. Measurements were made statically using the Faraday Cups. The measured Re and Os isotope ratios were oxide corrected offline. The data were corrected for fractionation. Analytical uncertainties are propagated and incorporate uncertainties related to Re and Os mass spectrometer measurements, blank abundances, and isotopic compositions, spike calibrations, and reproducibility of standard Re and Os isotope values. Procedural blanks conducted during the period of the molybdenite analysis are negligible relative to the Re and Os abundances measured in the samples (Re = 1.1 ± 0.3 ppt, Os = 0.5 ± 0.3 ppt, $^{187}Os/^{188}Os$ = 0.23 ± 0.05; n = 3). In-house reference solutions run during the analysis (Re Std. = 0.59763 ± 0.00108; DROsS = 0.16084 ± 0.00003; n = 3) are similar to long-term reproducibility data reported by Lawley and Selby (2012, and references therein). The Re-Os ages are presented as model ages from the simplified isotope equation [$t = ln(^{187}Os/^{187}Re + 1)/\lambda$], where t = model age, and λ = ^{187}Re decay constant and assumes no initial radiogenic Os. Inclusion of decay constant uncertainty and reporting of data with 2σ uncertainty allows for direct comparison of the Re-Os ages with the $^{40}Ar/^{39}Ar$ ages.

$^{40}Ar/^{39}Ar$ dating

Samples for in situ UVLAMP $^{40}Ar/^{39}Ar$ dating were prepared as doubly polished fluid inclusion wafers using the evolved approaches of Mark et al. (2005, 2006, 2008). Sericite for incremental step-heating was prepared using the methodology outlined in Mark et al. (2010b). Briefly, samples were crushed gently in a mortar and pestle and subjected to magnetic separation. The sericite-bearing fraction was run down a shaking table and a relatively pure sericite split collected. Subsequently clean grains were handpicked under a binocular microscope. All samples (wafers and separates) were cleaned in acetone and deionized water. They were parcelled in high-purity Al disks for irradiation. Standards Fish Canyon sanidine (28.02 ± 0.16 Ma, Renne et al., 1998), GA1550 biotite (98.79 ± 0.96 Ma, Renne et al., 1998) and Hb3gr hornblende (1073.57 ± 5.31 Ma, Jourdan et al., 2006) were loaded adjacent to the samples to permit accurate characterization of the neutron flux (J parameter). Samples were irradiated for 2,700 min in the Cd-lined facility of the CLICIT facility at the OSU TRIGA reactor. Standards were analyzed on a MAP 215-50 system (described below briefly and in more detail by Ellis et al., 2012)—Fish Canyon sanidine was analyzed by CO_2 laser total fusion as single crystals (n = 20), GA1550 (n = 20) was also analyzed by CO_2 laser total fusion, and Hb3gr was step-heated using a CO_2 scanning laser (n = 5; Barfod et al., 2014). Using GA1550 the J parameter was determined to a precision approaching 0.1% uncertainty. Using the J-parameter measurements from GA1550 ages were determined for Fish Canyon sanidine and Hb3gr. The ages overlapped at the 68% confidence (1σ) with the ages reported by Renne et al. (1998), showing the J parameters determined from GA1550 to be accurate.

Wafers were loaded into an ultra-high-vacuum (UHV) laser cell with an SiO_2 window. In situ UVLAMP Ar extraction was conducted using a New Wave UP-213-nm UV laser system (described in Moore et al., 2011). Raster pits, 50 × 50 × 5 μm^2 (amounts of ablated material approximately 1,250 μm^3) were made in mineral surfaces to extract the Ar isotopes. All gas fractions were subjected to 180 s of purification by exposure to two SAES GP50 getters (one maintained at room temperature, the other held at ca. 450°C). A cold finger was maintained at –95.5°C using a mixture of dry ice ($CO_{2[S]}$) and acetone. Ion beam intensities (i.e., Ar isotope intensities and hence ratios) were measured using a MAP 215-50 mass spectrometer in peak jumping mode. Measurements were made using a Balzers SEV-217 electron multiplier. The system had a measured sensitivity of 1.12 × 10^{-13} mol/V. The extraction and cleanup, as well as mass spectrometer inlet and measurement protocols and data acquisition were automated. Blanks (full extraction line and mass spectrometer) were made following every two analyses of unknowns. The average blank ± standard deviation (n = 28) from the entire blank run sequence was used to correct raw isotope measurements from unknowns. Mass discrimination was monitored by analysis of air pipette aliquots after every five analyses of unknowns (n = 13, 7.21 × 10^{-14} mol ^{40}Ar, $^{40}Ar/^{36}Ar$ = 289.67 ± 0.63).

The sericite separate was step-heated using a CO_2 laser (approx. 500°–1,500°C, optical pyrometer measurements). Extracted gases were subjected to 300 s of purification by exposure to two SAES GP50 getters (one maintained at room temperature, the other held at ca. 450°C). A cold finger was maintained at –95.5°C using a mixture of dry ice ($CO_{2[S]}$) and acetone. Ion beam intensities (i.e., Ar isotope intensities and hence ratios) were measured using a GVI ARGUS V noble gas mass spectrometer in "true" multicollection mode (Mark et al., 2009). Faraday cups (10^{11} ohm ^{40}Ar, 10^{12} ohm $^{39–36}Ar$) were used to make measurements. The system had a measured sensitivity of 7.40 × 10^{-14} mol/V. The extraction and cleanup, as well as mass spectrometer inlet and measurement protocols and data acquisition were automated. Blanks (full extraction line and mass spectrometer) were made following every two analyses of unknowns. The average blank ± standard deviation (n = 15) from the entire blank run sequence was used to correct raw isotope measurements from unknowns. Mass discrimination was monitored by analysis of air pipette aliquots after every five analyses of unknowns (n = 16, 7.32 × 10^{-14} moles ^{40}Ar, $^{40}Ar/^{36}Ar$ = 299.76 ± 0.23).

All Ar isotope data were corrected for backgrounds, mass discrimination, and reactor-produced nuclides and processed using standard data reduction protocols (e.g., Mark et al., 2005) and reported according to the criteria of Renne et al. (2009). The atmospheric argon isotope ratios of Lee et al. (2006), which have been independently verified by Mark et al. (2011b), were employed. The decay constants of Steiger and Jaeger (1977) were used as an intermediary step in the calculation of $^{40}Ar/^{39}Ar$ ages. The Berkeley Geochronology Center software (*MassSpec*) was used for data regression. $^{40}Ar/^{39}Ar$

ages presented relative to the standard ages of Renne et al. (1998) and the decay constants of Steiger and Jaeger (1977) include only analytical uncertainties (termed "analytical precision) reported at 2σ uncertainty level to allow for the internal comparison of our $^{40}Ar/^{39}Ar$ ages at the highest precision. Following determination of weighted average, $^{40}Ar/^{39}Ar$ ages for each sample of the data were reprocessed and ages were determined relative to the statistical optimization model of Renne et al. (2010, 2011) and are reported including full systematic uncertainties (termed "full external precision") at the 2σ level. This final step allows for accurate comparison of the $^{40}Ar/^{39}Ar$ and Re-Os ages using the most comprehensive set of physical constraints of any of the various $^{40}Ar/^{39}Ar$ calibrations in use today, as highlighted by Mark et al. (2014), Renne et al. (2013), and discussed in Renne et al. (2014). This approach is discussed further in the "Results" section below.

Results

All Re-Os isotope measurements are presented in Table 3 and the $^{40}Ar/^{39}Ar$ data are presented in Appendix File DM1.

Shear molybdenite, Re-Os

Data for sample A8406 (A and B) yield two Re-Os model ages that are indistinguishable (455.8 ± 5.5 and 454.1 ± 5.5 Ma, analytical precision only). The Re and ^{187}Os abundances for aliquots A and B are 1.6 and 3.5 ppm, and 7.5 and 16.7 ppb, respectively. The two analyses show variable abundances of Re and ^{187}Os owing to quartz contamination of aliquot A as discussed in the "Analytical Methods" section above. Aliquot B was a pure molybdenite separate. We have taken a weighted average of the two Re-Os ages (± analytical precision) and subsequently propagated the systematic decay constant uncertainty into the age data. The data yield a weighted average Re-Os age of 455.0 ± 3.9/4.4 Ma (2σ, analytical/full external precision).

Sample B1633 possessed a higher abundance of Re (15.2 ppm) and ^{187}Os (73.8 ppb). The sample yielded an Re-Os age of 459.1 ± 2.2/2.7 Ma (2σ, analytical/full external precision). Sample B1633 is indistinguishable at the 2σ level from the weighted mean Re-Os age of sample A8406.

Wall-rock clast-hosted muscovite in quartz veins, UVLAMP $^{40}Ar/^{39}Ar$

In situ laser ablation analyses (samples DAL 6A, DAL 6B, and DAL 49) of the muscovite within wall-rock clasts entrapped in the quartz veins (Fig. 15) yielded a normally distributed data population with an age of 455.2 ± 1.4 Ma (analytical precision, MSWD 1.2, n = 12; Fig. 17). All analyses had greater than 90% radiogenic ^{40}Ar ($^{40}Ar^*$). The data plotted on an isotope correlation plot yield an inverse isochron-data plot close to the x axis ($^{39}Ar/^{40}Ar$) and give an age that is indistinguishable from the weighted average age of the data population, but define a low-precision y axis reading that is indistinguishable from the atmospheric $^{36}Ar/^{40}Ar$ ratio (Lee et al., 2006).

Sericite in shears, UVLAMP $^{40}Ar/^{39}Ar$

Sericite in shears from within two quartz veins (samples DAL 42 and DAL 33) were analyzed using in situ UVLAMP $^{40}Ar/^{39}Ar$ dating (Fig. 16). Data yielded weighted average $^{40}Ar/^{39}Ar$ ages of 449.1 ± 4.0 Ma (analytical precision, MSWD 0.3, n = 6) and 449.4 ± 4.4 Ma (analytical precision, MSWD 0.5, n = 8), respectively. There was more atmospheric contamination in the shear sericite than the wall-rock muscovite, as evidenced by relatively low $^{40}Ar^*$ yields of between 50 and 80%. The lower $^{40}Ar^*$ yields however allowed for more spread of the data on the isotope correlation plots with both samples defining inverse isochrons with ages that are indistinguishable from the weighted average ages, and initial trapped components of atmospheric composition (Lee et al., 2006). The mean age from all analyses of sericite in the sheared quartz veins is 449.2 ± 3.0 Ma (analytical precision, MSWD 0.5, n = 13; Fig. 17).

Sericite in shears, incremental heating $^{40}Ar/^{39}Ar$

Sericite from the same shear as molybdenite in sample B1633 was incrementally step-heated. The data yield a plateau with greater than 80% ^{39}Ar (n = 7) and an age of 420.6 ± 1.4 Ma (analytical precision, MSWD 1.6; Fig. 18). The first two age steps step up from ca. 320 Ma to the plateau, suggesting that there has been some disturbance to the sample at this time. When cast on an isotope correlation plot the plateau steps define an inverse isochron with age indistinguishable from the plateau age and an initial trapped $^{40}Ar/^{36}Ar$ component indistinguishable from atmospheric argon ratios (Lee et al., 2006). Note that the plateau age is much younger than the coeval Re-Os age for this sample (discussed later).

$^{40}Ar/^{39}Ar$ ages relative to modern standard ages and decay constants (Renne et al., 2010, 2011)

The $^{40}Ar/^{39}Ar$ method is a relative dating technique with all ages referenced back to a standard of known age and decay constant. Renne et al. (2010, 2011) published an optimization model that used constraints from ^{40}K activity, K-Ar isotope data, and pairs of ^{238}U-^{206}Pb and $^{40}Ar/^{39}Ar$ data as inputs for estimating the partial decay constants of ^{40}K and $^{40}Ar^*/^{40}K$ ratio for Fish Canyon sanidine. This calibration has reduced systematic uncertainties (i.e., $^{40}Ar/^{39}Ar$ accuracy) to less than 0.25%. To present the most accurate ages for the dated samples and to produce Re-Os comparable $^{40}Ar/^{39}Ar$ data we have run all ages through the optimization model (the model spread sheet obtained directly from Paul Renne,

Table 3. Re-Os Data and Ages

Sample no.	Mass (g)	Re (ppm)	±2σ	^{187}Re (ppm)	±2σ	^{187}Os (ppb)	±2σ	Age (Ma)	±2σ (Ma)	±2σ (Ma) including decay constant
A8406B	0.024	1.57	0.01	0.99	0.01	7.54	0.07	455.8	5.5	5.7
A8406A	0.010	3.51	0.03	2.21	0.02	16.75	0.15	454.1	5.5	5.7
B1633	0.011	15.29	0.08	9.61	0.05	73.78	0.35	459.1	2.2	2.6

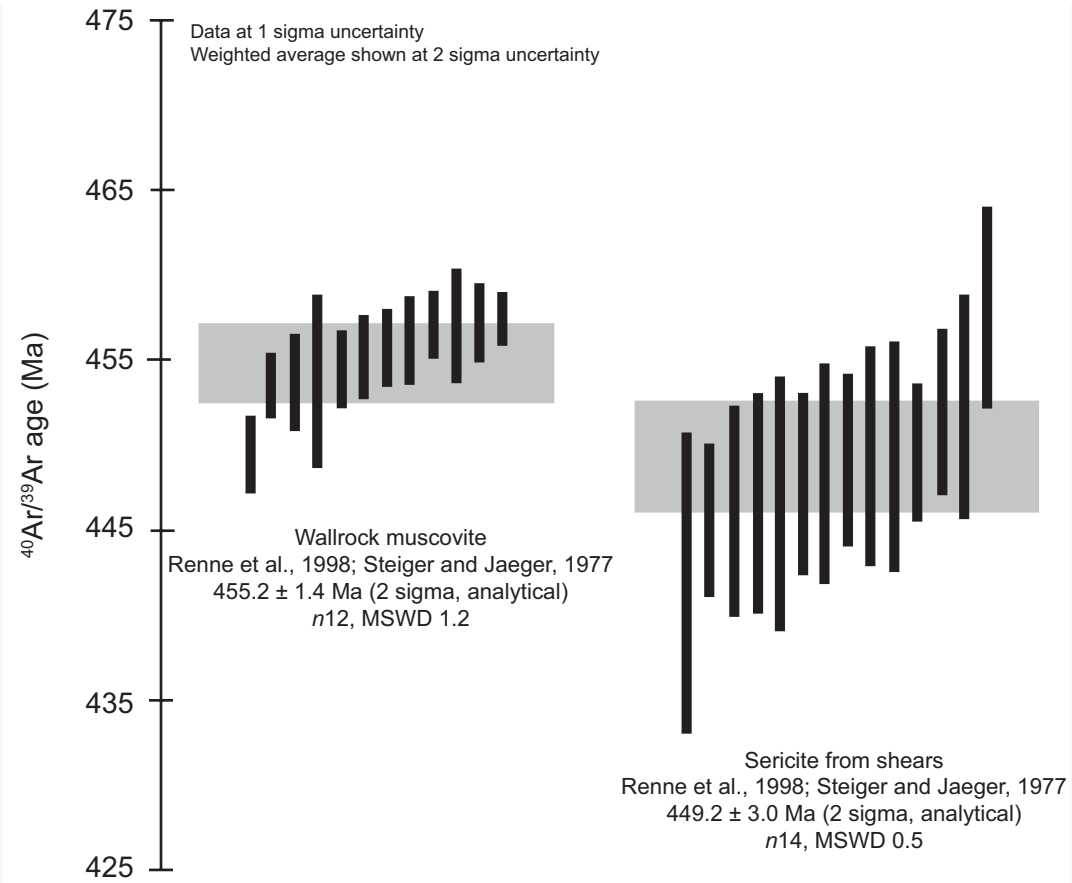

Fig. 17. Summary of $^{40}Ar/^{39}Ar$ age data for the muscovite from the wall-rock clast and the sericite from the shears. All $^{40}Ar/^{39}Ar$ age data reported at 2σ (analytical precision) using the decay constants of Steiger and Jaeger (1977) and the standard ages of Renne et al. (1998).

Berkeley Geochronology Centre). Data are reported at the 2σ uncertainty level as ± analytical/systematic uncertainties. The following ages are used throughout the remaining text. Their robustness and equivalence to the Re-Os ages are discussed below: Wall-rock muscovite (DAL 49 and DAL 6): 459.3 ± 2.8/3.4 Ma, sericite from shears (DAL 33 and DAL 42): 453.3 ± 3.0/3.6 Ma, and sericite from shear (B1633): 424.4 ± 2.8/3.8 Ma.

Discussion

Timing of terrane cooling through the muscovite T_c postpeak metamorphism

Most geochronological data for the Grampian event of the Caledonian orogeny in the British and Irish Caledonides comes from western Ireland and northeastern Scotland. Studies in western Ireland (closest to Curraghinalt) indicate that peak metamorphism and the main deformational episodes occurred during a brief period of time between ca. 475 to 465 Ma (e.g., Friedrich et al., 1999). High-temperature conditions lasted no longer than emplacement of the Oughterard granite which marks the end of Grampian magmatism in Connemara, western Ireland (U-Pb zircon: 463 ± 3 Ma) and thereafter the cooling history was relatively simple with surface temperatures being reached by ca. 443 Ma (Friedrich et al., 1999).

Friedrich et al. (1999) analyzed micas by $^{40}Ar/^{39}Ar$ dating, their data indicating that southern Connemara cooled from 460° to 350°C between 460 to 450 Ma. There is a large database of mica cooling ages from Connemara (Elias et al., 1988; Clift et al., 1996), the Ox Mountains in northwest Ireland (Flowerdew et al., 2000) and northeastern Scotland (Dempster, 1985; Dempster et al., 1995). Soper et al. (1999) noted that most of these fall in the range 465 to 440 Ma and provide further evidence of the regional cooling history. Closer to Curraghinalt a single $^{40}Ar/^{39}Ar$ biotite cooling age of 468 ± 1 Ma from the Tyrone Central inlier suggests that cooling was more rapid in this part of the orogen (Chew et al., 2008). At first inspection our wall-rock muscovite clast age (459.3 ± 2.8/3.4 Ma) agrees well with the cooling path for southern Connemara which, like Curraghinalt, is part of the Grampian terrane but is clearly different to that of the Tyrone Central inlier, which lies in the Midland Valley terrane (Fig. 19). We can envisage our $^{40}Ar/^{39}Ar$ data supporting one of two different scenarios.

Scenario 1: The simplest solution (Occam's Razor) and our favored interpretation is that the wall-rock mica $^{40}Ar/^{39}Ar$ age of 460 Ma from within the vein-supported clast is recording the time that the terrane cooled through the muscovite closure temperature of 400°C following peak metamorphism. This scenario provides a maximum age constraint to the gold

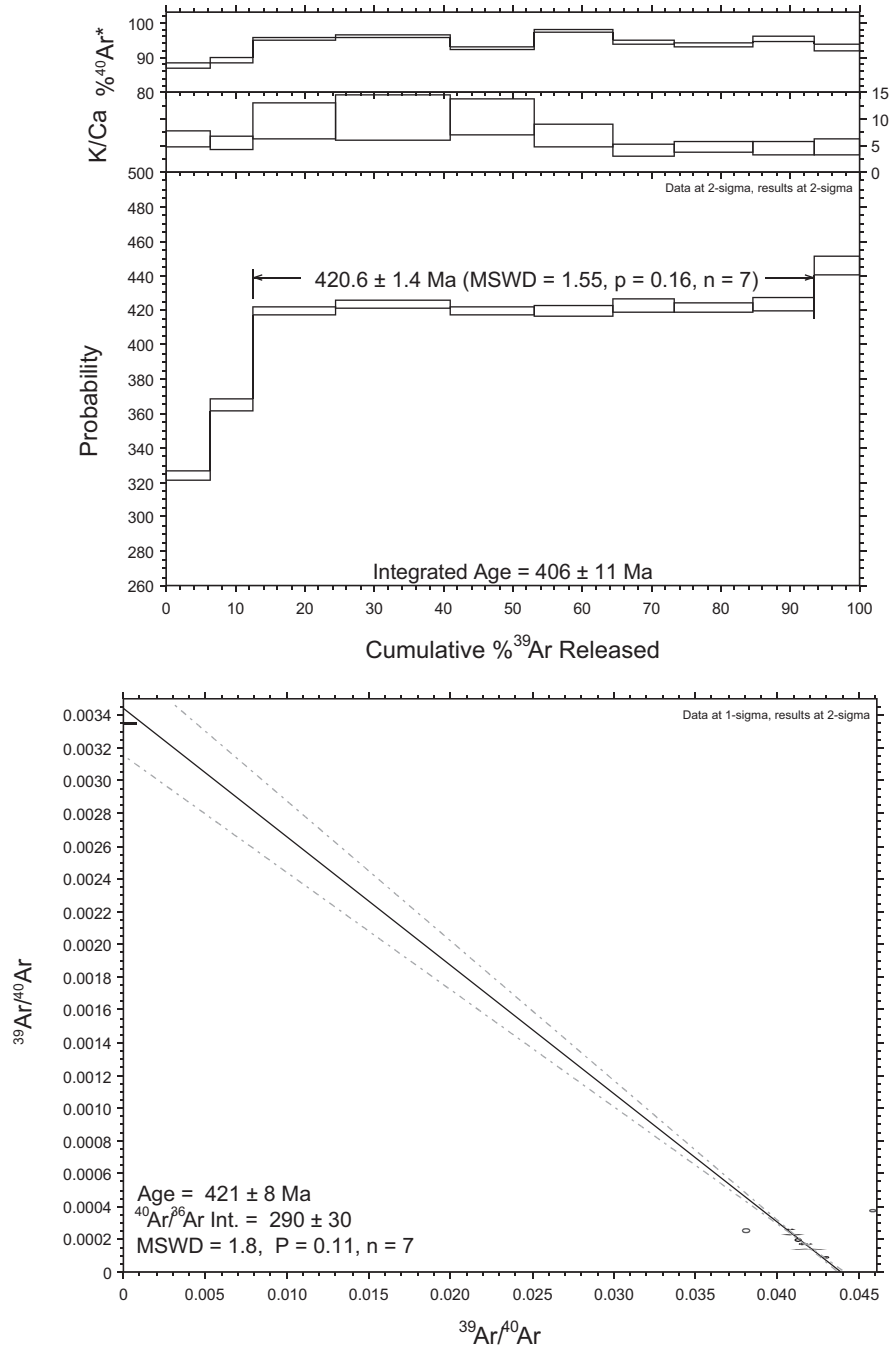

Fig. 18. $^{40}Ar/^{39}Ar$ step heating data for sample B1633. The data define a plateau age (>80% ^{39}Ar, n = 7) with steps composed of typically high radiogenic ^{40}Ar yields (>90% $^{40}Ar^*$). The data cast in an isotope correlation plot also define an inverse isochron with the x-intercept defining a $^{40}Ar/^{39}Ar$ age indistinguishable from the plateau age and a y-intercept $^{40}Ar/^{39}Ar$ composition that is indistinguishable from the modern-day atmosphere (Lee et al., 2006). All $^{40}Ar/^{39}Ar$ age data reported at 2σ (analytical precision), using the decay constants of Steiger and Jaeger (1977) and the standard ages of Renne et al. (1998). The data define a robust plateau age of 420.6 ± 1.4 Ma. The significance of this age is discussed within the text.

mineralization. We note for later discussion and in support of this scenario that the temperature for the wall rocks at ca. 460 Ma is close to that of the first generation of gold as determined by fluid inclusion data (Wilkinson et al., 1999; Parnell et al., 2000).

Scenario 2: Given that the metamorphic temperatures reached in southern Connemara (upper amphibolite facies) were higher than the Sperrin Mountains (upper greenschist facies), differences in the cooling histories could be expected. In this case we have to allow for the possibility that the terrane actually cooled to below the muscovite argon closure temperature before 460 Ma and it was the hot fluids associated with the first generation of gold mineralization that reset the $^{40}Ar/^{39}Ar$ age to ca. 460 Ma. This would

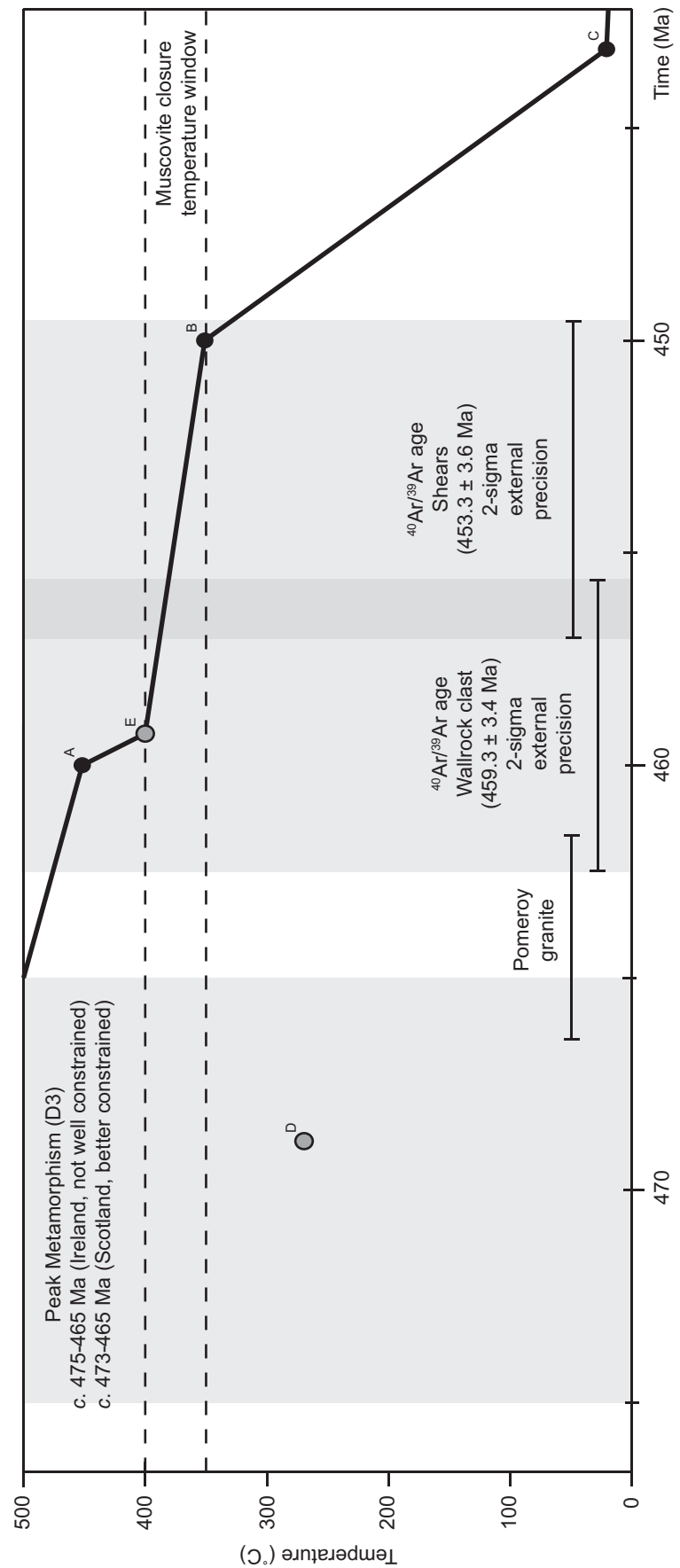

Fig. 19. Plot showing regional cooling trend reconstructed from previously published data. Peak metamorphism within the region was occurring between 475 to 465 Ma. The Pomeroy Granite (464 ± 2 Ma) is the youngest arc intrusion in the Tyrone Volcanic Group and marks the end of D_3 deformation. The data of Friedrich et al. (1999) show that at 460 Ma the terrane cooled from 450°C (A) to 350°C by 450 Ma (B). It is during this time interval that the terrane passed through the muscovite closure temperature (400°C) for the K-Ar system. By 443 Ma the terrane had cooled to surface temperatures (circle C; Friedrich et al., 1999). We show the biotite age of Chew et al. (2008). (D). Biotite has a closure temperature different from muscovite (280°C) and the age is unlikely to represent a regional terrane cooling age but does suggest that the Tyrone Igneous Complex has a radically different exhumation history to the adjacent Laurentian margin. Our $^{40}Ar/^{39}Ar$ age for the muscovite (ca. 459 Ma) from the wall-rock clasts appears consistent with the data of Friedrich et al. (1999), which suggests that the Curraghinalt region passed through the muscovite closure temperature between 460 to 450 Ma.

mean that our $^{40}Ar/^{39}Ar$ age for the wall-rock mica within the vein-supported clast actually dates the first generation of gold mineralization. The combination of the maximum temperature (400°C) reached and the likely maximum duration of the fluid-driven thermal pulse (Q2, 0.1–1 Ma, which is based on the cooling time of a small single-phase pluton and the duration of a mesothermal orogenic hydrothermal system; Cathles et al., 1997; Weatherly and Henley, 2013) would have impacted the Ar systematics of the muscovite. To interrogate this we have run a series of DIFFARG models (Wheeler, 1996; Mark et al., 2008) to show the effect of a 400°C pulse of 0.1, 0.5, and 1 Ma duration (covering all likely worst-case scenarios for the duration of the mineralization episode) on the age of a 460 Ma muscovite crystal with an appropriately defined effective diffusion dimension. We measured some of the muscovite crystals (Fig. 14B). The width of the crystals (short axes) ranges from 10 to 30 μm with an average of around 20 μm. For a 20-μm-sized muscovite crystal (i.e., effective diffusion dimension of 20 μm) exposed to a 400°C pulse for 0.1, 0.5, and 1 Ma, the $^{40}Ar/^{39}Ar$ ages are completely reset (Fig. 20). In fact, exposure to this temperature for less than 0.01 Ma actually resets the system fully.

Although plausible scenario 2 requires reheating of the region by pulsing of hot fluids through the fault-fracture system shortly after cooling from temperatures in excess of 500°C (upper greenschist facies), and we feel there is no need to invoke such a mechanism at this time given the coincidence between muscovite closure temperature, terrane temperature, and fluid inclusion data detailed in scenario 1. It is important to note that although we favour scenario 1, both scenarios effectively yield a maximum age for the first generation of gold mineralization.

Combined $^{40}Ar/^{39}Ar$ and Re-Os age for the sericite-molybdenite shears

The Re-Os and $^{40}Ar/^{39}Ar$ ages for the molybdenite and sericite, respectively, from samples DAL 33, DAL 42, A8406 A-B, and B1633 are equivalent at the 2σ uncertainty level. Therefore, we have determined a combined Re-Os and $^{40}Ar/^{39}Ar$ age for the sericite-molybdenite shears by calculating the mean age ± standard deviation (reported at the 2σ uncertainty level). The combined age is 455.8 ± 3.0 Ma (allowing for all sources of random and systematic uncertainty).

Significance of age data to timing and duration of mineralization

As discussed above, the most likely interpretation of our clast-hosted muscovite age is that it represents a regional cooling age and provides a maximum age for the first generation of gold mineralization. The age of the third and last generation of gold mineralization is provided by the combined Re-Os and $^{40}Ar/^{39}Ar$ ages, which yield a weighted average age of 455.8 ± 3.0 Ma for sericite and molybdenite coexisting with electrum in microshears cutting the first two generations of gold mineralization. This age further provides a minimum age constraint for the first two generations of gold mineralization, which includes the main gold resource and constrains the maximum possible duration of mineralization to a window of ca. 10 Ma (i.e., 462.7–452.8 Ma; Fig. 21).

Temporal correlations between mineralization and regional events

These new chronological data show that mineralization closely followed the end of the main tectonomagmatic events (ca. 465 Ma) of the Grampian event of the Caledonian orogeny (Fig. 22). There is good evidence that at this time uplift, exhumation and orogenic extensional collapse were taking place in the Sperrin Mountains and elsewhere in the British and Irish Caledonides. Mica $^{40}Ar/^{39}Ar$ cooling ages from the British and Irish Caledonides have been interpreted to support rapid exhumation and cooling of the nappe pile (Friedrich et al., 1999; Soper et al., 1999; Flowerdew et al., 2000). Collapse of the orogen soon after peak metamorphism and main-stage deformation is indicated by extensional structures in the Sperrin Mountains that can be traced for at least 100 km along strike into southern Donegal (Alsop and Hutton, 1993a) and detachment faulting in western Ireland (Clift et al., 2004). Simultaneously, Dalradian sediments in Connemara were rapidly exhumed, possibly at rates of at least 0.7 km/Ma (Power et al., 2001). The radioisotopic ages obtained herein from a well-characterized paragenetic sequence indicate that the main gold resource at Curraghinalt was emplaced during this regional extensional regime, as originally envisaged by Alsop and Hutton (1993a). It has been proposed that the vein-filling structures were formed during compressional movements on the Omagh thrust over a footwall ramp (Parnell et al., 2000). However, the timing of mineralization indicates that the vein structures were more likely formed as the ramp area became a zone of extension during hanging-wall collapse.

There is no well-documented magmatism in the Sperrin Mountains or northern Ireland that spans the interval of mineralization (462.7–452.8 Ma) or correlates with the precisely determined timing for the third phase of mineralization. However, there is an overlap between the upper end of this interval and the youngest (464 ± 2 Ma) intrusion (Pomeroy granite) of a suite of arc-related Tyrone Volcanic Group plutons (Cooper et al., 2008, 2011; Hollis et al., 2012, 2013b; Figs. 1, 21). Therefore, it is conceivable that subduction-related activity may have continued beyond ca. 464 Ma in the Tyrone arc after it was over-ridden by the Laurentian margin (Earls et al., 1996). Farther afield (200 km from Curraghinalt) in the orogen, there is magmatism that correlates with the window of mineralization. The Oughterard granite in western Ireland has been dated at ca. 462 Ma (Friedrich et al., 1999) and in northeast Scotland the S-type Kennethmont granite has been dated at ca. 458 Ma (Oliver, 2001).

There is a clustering of Rb-Sr pegmatite ages ca. 455 Ma in the Ox Mountains in northwestern Ireland and the Tyrone Central inlier (Flowerdew et al., 2000; Chew et al., 2008) but the significance of these is uncertain owing to problems interpreting Rb-Sr ages. Those in the former area may represent resetting due to a later regional fluid circulation event (M. J. Flowerdew, pers. commun.). This interpretation could be applied to the latter and may be linked to a late orogenic switch from compressional to extensional tectonics (discussed below). Despite some doubt about the exact age of the pegmatites there is a spatial and likely genetic connection between their intrusion and late orogenic crustal extension (Alsop and Hutton, 1993a; Flowerdew et al., 2000).

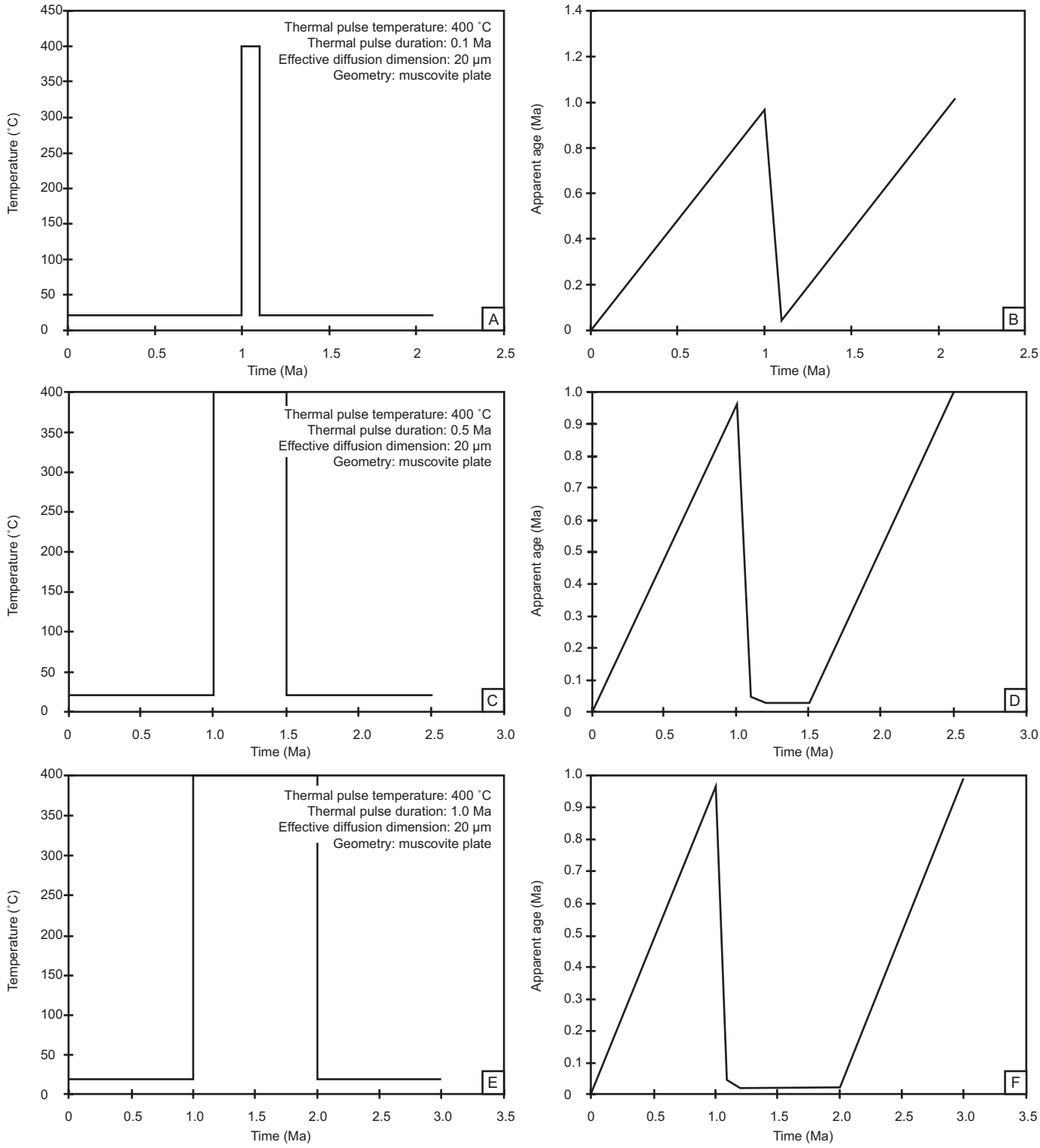

Fig. 20. Series of Ar diffusion (DIFFARG) models showing the impact of different thermal pulses of different duration on the $^{40}Ar/^{39}Ar$ age for the muscovite crystals. Note that for all scenarios following a 400°C thermal pulse the $^{40}Ar/^{39}Ar$ system is reset for all scenarios (0.1, 0.5, and 1 Ma). Following the resetting event radiogenic ^{40}Ar begins to accumulate again from the decay of ^{40}K. Note DIFFARG is a forward modeling program and as such the model runs forward in time and not backward (see Mark et al., 2008, for further details).

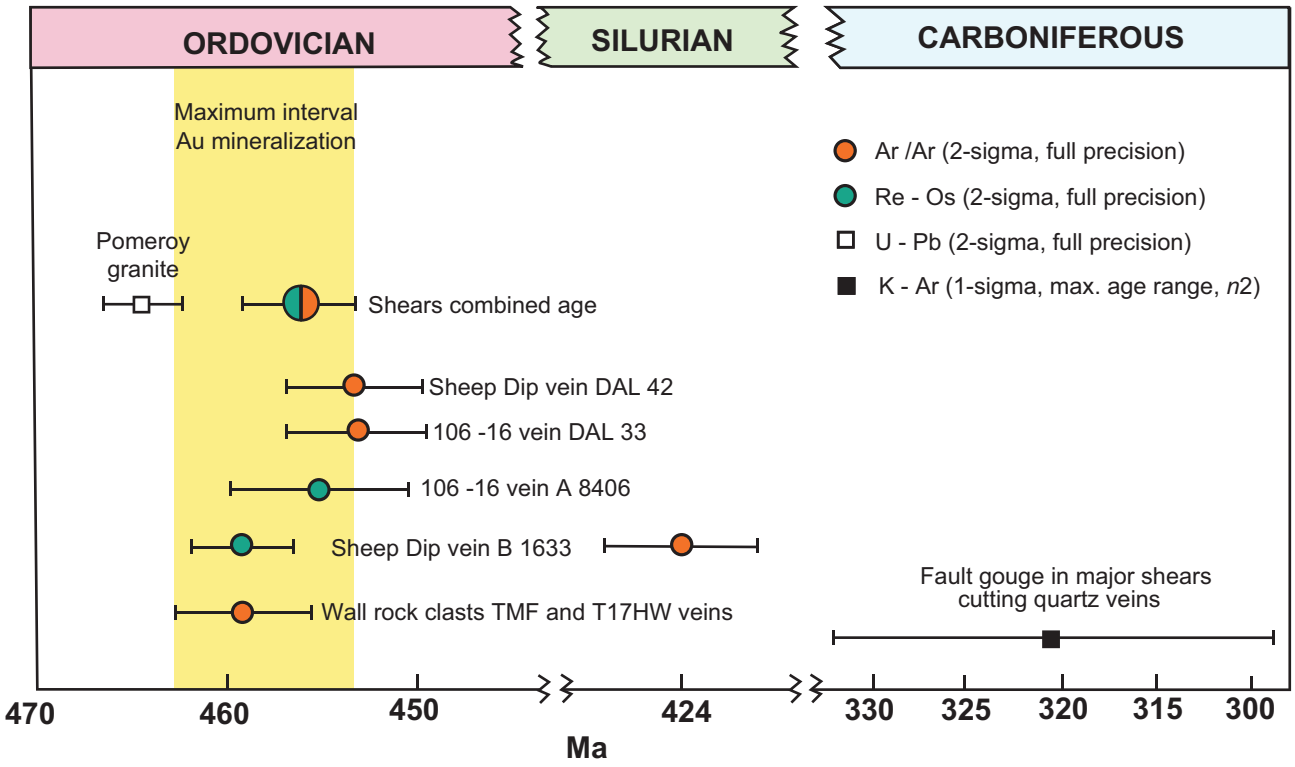

Fig. 21. Summary of the $^{40}Ar/^{39}Ar$ and Re-Os data from this study and including the interval of gold mineralization at Curraghinalt. The maximum possible interval of gold mineralization is constrained by the age of the wall-rock clasts and the age of the sericite- and molybdenite-bearing microshears. The D_3 deformed Pomeroy Granite also provides a maximum age constraint on the mineralization (data from Cooper et al., 2011). Minimum (Carboniferous) ages are given by K-Ar ages obtained on fault gouge from two major shears (Crows Foot and Kiln, Fig. 4A) which transect the auriferous quartz veins (data from Earls et al., 1996). The K-Ar age shown is the average and maximum range of the two K-Ar ages presented by Earls et al. (1996). The $^{40}Ar/^{39}Ar$ data are reported relative to the optimization model of Renne et al. (2011) and include all sources of uncertainty.

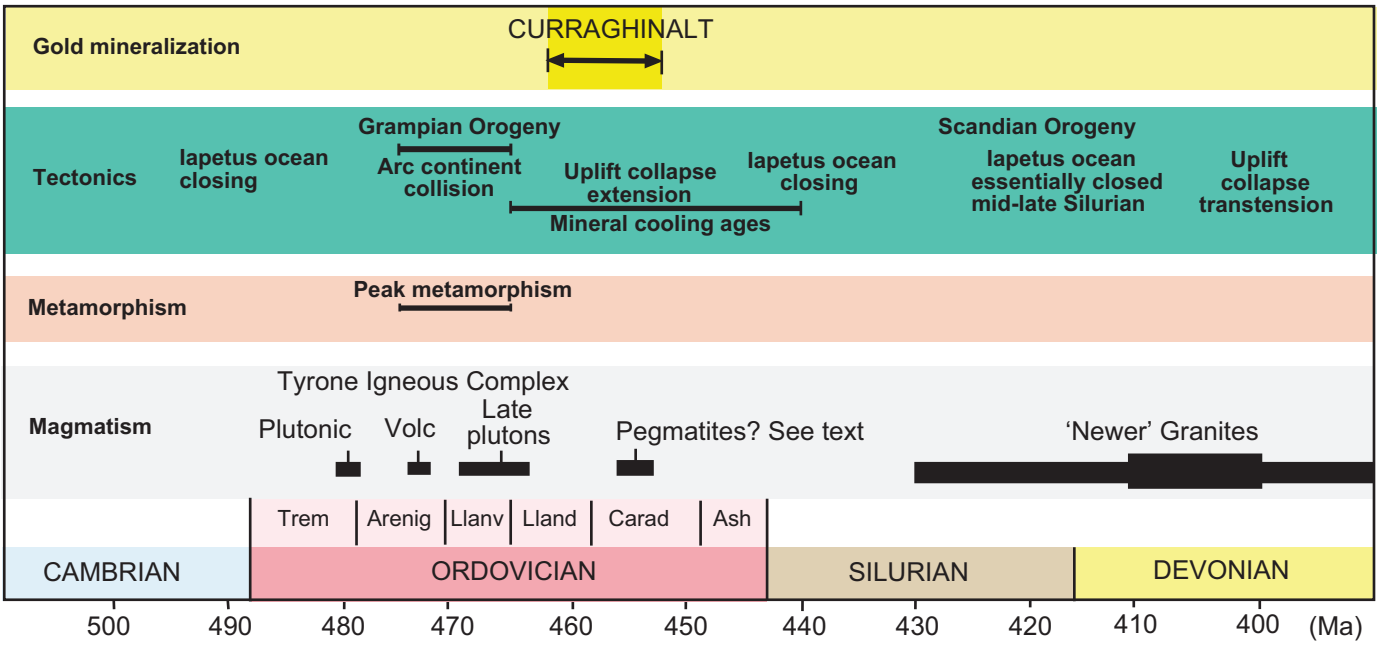

Fig. 22. Timelines showing the maximum interval of gold mineralization at Curraghinalt in relation to some major tectonic, magmatic, and metamorphic events in the Caledonian orogen of northern Britain. The $^{40}Ar/^{39}Ar$ data are reported relative to the optimization model of Renne et al. (2011) and include all sources of uncertainty.

Sedimentation was occurring in the Pomeroy forearc basin that bounded the accreted Tyrone Igneous Complex by the Late Ordovician and possibly earlier (Cooper and Mitchell, 2004). The sediments are exposed only in a small inlier about 25 km southeast of Curraghinalt (Fig. 1) and so the full areal and stratigraphic extent of the basin is unknown. The oldest known sediments belong to the Soudleyan substage (ca. 454–452 Ma; Mitchell, 1977), which overlaps with the lower end of the mineralization interval.

Sources of fluids, heat, metals, and sulfur in the Curraghinalt mineralizing system

Using two independent geochronological systems in conjunction with a detailed reappraisal of the paragenesis, this study has established that all three generations of gold mineralization at Curraghinalt were deposited in the Late Ordovician (462.7–452.8 Ma) at a time of uplift, exhumation, and regional extension of the Grampian orogenic belt. Armed with these new radioisotopic ages and observations and data from previous studies we now reexamine some existing theories regarding the sources of heat, fluids, metals, and sulfur in the mineralizing system.

Fluids and heat

We cannot rule out the involvement of magmatic fluids in the first generation of gold mineralization (Parnell et al., 2000) but there is an alternative scenario that we consider more plausible. The case for a magmatic fluid rests on fluid inclusion data that identified a fluid with a generally higher temperature (<420°C), higher salinity (10 wt % NaCl + KCl equiv), and low CO_2 content (ca. 15 wt %) than typical metamorphic fluids (Parnell et al., 2000). However, metamorphic or highly exchanged meteoric fluids with these characteristics could have been generated in the geologic setting identified in this study. For example, deeply penetrating meteoric fluids with similar temperatures have been described from the Southern Alps in New Zealand (Menzies et al., 2014), where there is no known igneous activity. The unusually high temperatures found at a shallow level here were likely achieved as a result of rapid uplift bringing hot rocks close to the surface.

A similar situation may have prevailed in the Irish segment of the Grampian orogenic belt at this time where high uplift rates are indicated by a concentration of mica cooling ages (above) and by fluid inclusion data, suggesting uplift rates of at least 0.7 km/Ma (Power et al., 2001). Considering scenario 1 for the $^{40}Ar/^{39}Ar$ data presented above, we also know that the crust was hot (close to 400°C, muscovite argon closure temperature) at the time of mineralization and therefore capable of producing crustal fluids at a similar temperature to the first generation of gold. It is also possible that the underlying arc was still hot given that the age of the youngest known arc-related granite at ca. 464 Ma overlaps within uncertainties the age of mineralization (Fig. 21) and provided an important heat source during the mineralization interval.

These considerations offer an alternative explanation for the unusual combination of high temperatures and shallow emplacement depth found at Curraghinalt (trapping pressures mainly <1 kb and epithermal vein textures are consistent with an emplacement depth of <10 km, Parnell et al., 2000). Also, since metamorphic dehydration reactions may be driven by late orogenic rapid uplift (Yardley and Cleverly, 2013) hot CO_2-rich metamorphic fluids might be anticipated at similar shallow depths and mixing of these with meteoric fluids could generate the CO_2 levels observed in the Curraghinalt fluids. Furthermore the moderate fluid salinities found in the Q2 mineralization (Wilkinson et al., 1999) could be generated by metamorphism of the Dalradian sediments. Shelf sediments, such as those in the Dalradian sequence, can yield fluids with salinities similar to those seen at Curraghinalt (Yardley and Graham, 2002).

In contrast to these fluids, the sources of the fluids for the second generation of gold are well constrained and involve a mixture of formation waters and basinal brines (Wilkinson et al., 1999). However, these fluids are of Ordovician rather than Carboniferous age as proposed by Wilkinson et al. (1999). The source of the basinal fluids is unknown but they may have been derived from a forearc basin, such as that occurring at Pomeroy to the southeast of Curraghinalt (Fig. 1). Another possibility is that the brines were squeezed from the overridden Tyrone Volcanic Group by compression (e.g., Mark et al., 2007). This could explain the abundance of Cu in this generation of mineralization. The east-west shears at Curraghinalt (Fig. 4) are possible fluid conduits for migration of such brines.

The origin of the fluids responsible for Q1 and the sericite- and molybdenite-bearing microshears is poorly constrained at present. A metamorphic fluid has been suggested for Q1 (Parnell et al., 2000).

The timing of the hydrothermal activity broadly coincides with the switch from compression to extension during orogenic collapse and this may have triggered the release of gold-bearing fluids (Alsop and Hutton, 1993a). At Curraghinalt this was reflected in a switch from SE-directed compressional movements on the Omagh thrust to NW-directed hanging-wall collapse and perhaps also the strike-slip faulting responsible for the formation of the gold vein-hosting structures. It is a common feature of hydrothermal systems that the shift from high-angle reverse to strike-slip faulting is favorable for a high fluid flux and mineralization (e.g., Goldfarb et al., 1991).

Metals and sulfur

Published S and Pb isotope data are consistent with the underlying Tyrone volcanic arc being not only a source of heat and fluids as discussed above but also S and Pb by leaching (Parnell et al., 2000; Standish et al., 2014). These elements could be derived from the widespread precious and base metal enrichments and volcanogenic massive sulfide and porphyry-style mineralization hosted by the arc (Clifford et al., 1992; Hollis et al., 2014). There is also isotopic evidence that some of the Pb may have been derived from the Dalradian metasediments hosting the mineralization (Standish et al., 2014). The enrichments of Mo, Bi, and Te at Curraghinalt suggest the involvement of granitic rocks in the metal reservoir and a possible source, again by leaching, are the abundant granites in the Tyrone Igneous Complex. Differences in the mineralogy between the three generations of gold mineralization (Fig. 5) may be attributed in part to changes in the metal reservoirs. Such changes would be expected in an active tectonic setting and might include episodic movements along the Omagh thrust, allowing access to different portions of the Tyrone Igneous Complex.

Evidence for post-Ordovician activation of fault structures

The age of 424.4 ± 2.8/3.6 Ma obtained for fine-grained sericite in sample B1633 is notably younger than the coeval molybdenite dated at 459.1 ± 2.2/2.7 Ma from the same sample. There is localized magmatic activity (trachy-andesite dikes) occurring at this time within the western Sperrin Mountains (Cooper et al. 2013) but this localized magmatic activity is unlikely to have disturbed the $^{40}Ar/^{39}Ar$ system in our samples as the nearest known dike is more than 10 km from Curraghinalt. However, it is possible that later fault movements have disturbed the $^{40}Ar/^{39}Ar$ system in sample B1633 with the age of 424.4 ± 2.8/3.6 Ma correlating broadly with final mid-Silurian closure of the Iapetus Ocean in northern Ireland (Chew and Stillman, 2009; Cooper et al., 2013). Possibly the stresses set up by the collision reactivated some of the shears and induced a grain-size reduction of the sericite. Grain- size reduction is known to reset the $^{40}Ar/^{39}Ar$ system and could be responsible for the younger $^{40}Ar/^{39}Ar$ age seen in this sample (Henderson et al., 2011). The coeval molybdenite dated at 459.1 ± 2.2/2.7 Ma is unlikely to have been affected by this process, partly due to the high closure temperature of the Re-Os system in molybdenite (Suzuki, 1996; Selby et al., 2002).

The $^{40}Ar/^{39}Ar$ step-heating spectrum for sample B1633 (Fig. 18) also shows a disturbance at ca. 320 Ma. This age is close to fault gouge K-Ar ages (ca. 315 and ca. 325 Ma, Fig. 21) in the area reported by Earls et al. (1966) and Parnell et al. (2000), lending support to the suggestion that these fault structures were reactivated during the Variscan orogeny.

Is Curraghinalt an orogenic gold deposit?

Given that Curraghinalt may not be intrusion related, we consider whether it is an orogenic gold deposit as defined in Goldfarb et al. (2005). The following features support this alternative classification. The ore grade is high. It shows a close association with a convergent plate margin. It postdates peak metamorphism and was emplaced into rocks affected by greenschist facies metamorphism during the later stages of still ongoing regional deformation. The temperature, salinity, and CO_2 content of the fluids responsible for the main gold resource are within the ranges attributed to these deposits (Goldfarb et al., 2005), as is the metal assemblage of As, Bi, Sb, and Te (although W is lacking). Nevertheless, there are some unusual features: (1) the combination of a high temperature and shallow depth of emplacement, which, in the absence of an obvious magmatic source, is likely explained by a rapid rate of uplift (2) the Cu content is high but this is linked mainly to the later incursion of basinal brines rather than the fluids responsible for the main gold resource; and (3) the enrichments of Mo, Bi, and Te are more typical of intrusion-related gold deposits but could be explained in this case by leaching of granites in the underlying Tyrone island arc. We conclude that these unusual features can be explained by the geologic setting and that Curraghinalt is probably an orogenic gold deposit.

A genetic model for Curraghinalt

Many aspects of the Curraghinalt mineralization such as the mineralogy, geochemistry, fluid composition, and structural controls that are crucial for developing robust genetic models have been established by previous studies (Earls et al., 1996; Wilkinson et al., 1999; Parnell et al., 2000). The main contributions of this study toward understanding the genesis of Curraghinalt have been to refine the paragenesis and, more importantly through dating of the mineralization, to establish precisely its regional geologic setting. From these data a conceptual genetic model may be constructed for Curraghinalt, which can be used to inform exploration programs for similar gold deposits in the Caledonides and collision zones elsewhere.

The salient features of the setting are the following: (1) a collision zone where a continental margin has been obducted over an island arc; (2) following rapid late orogenic uplift the crustal profile at Curraginalt during the mineralization interval consisted of a thick sequence of metasediments overlying a still hot and fertile (mineralized) arc; and (3) subsequent orogenic collapse and extension resulted in increased crustal permeability. This created an ideal setting for developing large and long-lasting hydrothermal systems and the emplacement of metalliferous mineralization, i.e., multiple sources of heat, fluids, and metals in the arc and an overlying permeable crust charged with crustal orogenic fluids where fluid mixing and precipitation of metals could occur. This ideal setting may explain why Curraghinalt is the largest known gold deposit in the British and Irish Caledonides.

Conclusions

A third and new generation of gold mineralization has been identified at Curraghinalt occurring in microshears cutting the first two phases of gold-sulfide mineralization. The shears contain mainly sericite with minor pyrite and molybdenite, trace electrum, and a BiAg telluride.

All gold mineralization at Curraghinalt formed in the ca. 10 Ma interval (462.7–452.8 Ma) during the Late Ordovician. It closely followed peak metamorphism associated with the Grampian event of the Caledonian orogeny and is temporally linked with an extensional setting following orogenic uplift and collapse.

The late orogenic setting offers an alternative classification for the mineralization and we suggest that Curraghinalt is more likely an orogenic- rather than intrusion-related gold deposit. In the former scenario crustal orogenic fluids are alternatives to magmatic fluids and rapid uplift could explain the unusual combination of high temperatures and shallow emplacement of the first generation of mineralization at Curraghinalt. Brines occurring in ore fluids responsible for the second generation of mineralization may have been sourced from the Tyrone Igneous Complex or from a nearby forearc basin.

Data from this and previous studies are consistent with a genetic model whereby a combination of the extensional setting, rapid uplift, and a hot island arc underlying a thick sequence of metasediments favored the formation of large, long-lasting hydrothermal systems with metals, sulfur, and fluids derived in part from the arc.

This study highlights the importance of obtaining precise geochronological data for vein-hosted gold mineralization at an early stage of a study so that its geologic setting can be accurately identified and a robust genetic model constructed.

Acknowledgments

We are grateful to Dalradian Gold Ltd. for providing the sections for petrographic analysis, geochemical data, and general support. We would also like to thank the following: John Still, Alison Sandison, and Jenny Johnston of the School of Geosciences, University of Aberdeen, for assistance with the SEM studies (JS) and with preparing figures (AS and JJ); NERC for ongoing funding of the Argon Isotope facility at SUERC; Jim Imlach and Ross Dymock at SUERC for technical assistance; and Martin Lee at the School of Geographical and Earth Sciences at the University of Glasgow for use of the SEM/CL equipment. The paper has benefitted significantly from comments by the official reviewers and unofficial reviews by Garth Earls, Jamie Wilkinson, Mark Cooper, and Adrian Boyce, and detailed conversations with Ian Alsop (structural geology of the Sperrins) and Nyree Hill and Gawen Jenkin (gold mineralization in the Caledonides). The authors are entirely responsible for the conclusions expressed.

REFERENCES

Alsop, G.I., and Hutton, D.H.W., 1993a, Caledonian extension in the north Irish Dalradian: Implications for the timing and activation of gravity collapse: Journal Geological Society of London, v. 150, p. 33–36.

——1993b, Major southeast-directed Caledonian thrusting and folding in the Dalradian rocks of mid-Ulster: Implications for Caledonian tectonics and mid-crustal shear zones: Geological Magazine, v. 130, p. 233–244.

Barfod, D.N., Mark, D.F., Tait, A., Dymock, R.C., and Imlach, J., 2014, Argon extraction from geological samples by CO_2 scanning laser step-heating: Geological Society of London Special Publication 378, p. 79–90.

Cathles, L.M., Erendi, A.H., and Barrie, T., 1997, How long can a hydrothermal system be sustained by a single intrusive event?: Economic Geology, v. 92, p. 766–771.

Chew, D.M., and Stillman, C.J., 2009, Late Caledonian orogeny and magmatism, *in* Holland C.H., and Sanders, I.S., eds., The geology of Ireland, 2nd ed.: Edinburgh, Scotland, Dunedin Academic Press, p. 143–173.

Chew, D.M., Flowerdew, M.J., Page, L.M., Crowley, Q.G., Daly, J.S., Cooper, M.R., and Whitehouse, M.J., 2008, The tectonothermal evolution and provenance of the Tyrone Central inlier, Ireland: Grampian imbrication of an outboard Laurentian microcontinent?: Journal Geological Society of London, v. 165, p. 675–685.

Clifford, J.A., Earls, G., Meldrum, A.H., and Moore, N., 1992, Gold in the Sperrin Mountains, northern Ireland: An exploration case history, *in* Bowden, A.A., Earls, G., O'Connor, P.G., and Pyne, J.F., eds., The Irish minerals industry 1980–1990: Dublin, Irish Association for Economic Geology, p. 77–87.

Clift, P.D., Yardley, B.W.D., and Bussy, F., 1996, U-Pb and Rb-Sr geochronology of Connemara, western Ireland: Journal Geological Society of London, v. 153, p. 109–120.

Clift, P.D., Dewey, J.F., Draut, A.E., Chew, D.M., Mange, M., and Ryan, P.D., 2004, Rapid tectonic exhumation, detachment faulting and orogenic collapse in the Caledonides of western Ireland: Tectonophysics, v. 384, p. 91–113.

Cooper, M.R., and Johnston, T.P., 2004, Central Highlands (Grampian) terrane-metamorphic basement, *in* Mitchell, W.I., ed., The geology of northern Ireland: Geological Survey of Northern Ireland, p. 9–24.

Cooper, M.R., and Mitchell, W.I., 2004, Midland Valley terrane, *in* Mitchell, W.I., ed., The geology of northern Ireland: Geological Survey of Northern Ireland, p. 25–40.

Cooper, M.R., Crowley, Q.G., and Rushton, A.W.A., 2008, New age constraints for the Ordovician Tyrone Volcanic Group, northern Ireland: Journal Geological Society of London, v. 165, p. 333–339.

Cooper, M.R., Crowley, Q.G., Hollis, S.P., Noble, S.R., Roberts, S., Chew, D., Earls, G., Herrington, R., and Merriman, R.J., 2011, Age constraints and geochemistry of the Ordovician Tyrone Igneous Complex, northern Ireland: Implications for the Grampian orogeny: Journal Geological Society of London, v. 168, p. 837–850.

Cooper, M.R., Crowley, Q.G., Hollis, S.P., Noble, S.R., and Henney, P.J., 2013, A U-Pb age for the Late Caledonian Sperrin Mountains minor intrusions suite in the north of Ireland: Timing of slab break-off in the Grampian terrane and the significance of deep-seated, crustal lineaments: Journal Geological Society of London, v. 170, p. 603–614.

Creaser, R.A., Papanastassiou, D.A., and Wasserburg, G.J., 1991, Negative thermal ion mass spectrometry of osmium, rhenium and iridium: Geochimica et Cosmochimica Acta, v. 55, p. 397–401.

Dempster, T.J., 1985, Uplift patterns and orogenic evolution in the Scottish Dalradian: Journal Geological Society of London, v. 142, p. 111–128.

Dempster, T.J., Hudson, N.F.C., and Rogers, G., 1995, Metamorphism and cooling of the NE Dalradian: Journal Geological Society of London, v. 152, p. 383–390.

Dewey, J.F., 2005, Orogeny can be very short: Proceedings of the National Academy of Sciences of the United States of America, 102, 15286–15293, doi: 101073/pnas 0505516102.

Earls, G., Hutton, D.W.H., Wilkinson, J.J., Moles, N., Parnell, J., Fallick, A.E., and Boyce, A.J., 1996, The gold metallogeny of northwest Northern Ireland: Geological Survey of Northern Ireland Technical Report 96/6, 107 p.

Elias, E.M., Macintyre, R.M., and Leake, B.E., 1988, The cooling history of Connemara, western Ireland, from K-Ar and Rb-Sr age studies: Journal Geological Society of London, v. 145, p. 649–660.

Ellis, B.S., Mark, D.F., Pritchard, C.J., and Wolff, J.A., 2012, Temporal dissection of the Huckleberry Ridge tuff using the $^{40}Ar/^{39}Ar$ dating technique: Quaternary Geochronology, v. 9, p. 34–41.

Flowerdew, M.J., Daly, J.S., Guise, P.G., and Rex, D.C., 2000, Isotopic dating of overthrusting, collapse and related granitoid intrusion in the Grampian orogenic belt, northwestern Ireland: Geological Magazine, v. 137, p. 419–435.

Friedrich, A.M., Hodges, K.V., Bowring, S.A., and Martin, M.W., 1999, Geochronological constraints on the magmatic, metamorphic, and thermal evolution of the Connemara Caledonides, western Ireland: Journal Geological Society of London, v. 156, p. 1217–1230.

Goldfarb, R.J., Snee, L.W., Miller, L.D., and Newberry, R.J., 1991, Rapid dewatering of the crust deduced from ages of mesothermal gold deposits: Nature, v. 354, p. 296–299.

Goldfarb, R.J., Baker, T., Dube, B., Groves, D.I., Hart, C.J.R., and Gosselin, P., 2005, Distribution, character, and genesis of gold deposits in metamorphic terranes: Economic Geology 100th Anniversary Volume, p. 407–450.

Harrison, T.M., Celerier, J., Aikman, A.B., Herman, J., and Heizler, M.T., 2009, ^{40}Ar diffusion in muscovite: Geochimica et Cosmochimica Acta, v. 73, p. 1039–1051.

Henderson, A.L., Najman, Y., Parrish, R., Mark, D.F., and Foster, G.L., 2011, Constraints on the timing of India-Eurasia collision; a re-evaluation of evidence from the Indus Basin sedimentary rocks of the Indus-Tsangpo suture zone, Ladakh, India: Earth Science Reviews, v. 106, no. 3–4, p. 265–292, doi:10.1016/j.earscirev.2011.02.006.

Hollis, S.P., Roberts, S., Cooper, M.R., Earls, G., Herrington, R.J., Condon, D.J., Cooper, M.R., Archibald, S.M., and Piercey, S.J., 2012, Episodic-arc ophiolite emplacement and the growth of continental margins: Late accretion in the northern Irish sector of the Grampian-Taconic orogeny: GSA Bulletin, v. 124, p. 1702–1723.

Hollis, S.P., Cooper, M.R., Roberts, S., Earls, G., Herrington, R., and Condon, D.J., 2013a, Evolution of the Tyrone ophiolite, Northern Ireland, during the Grampian-Taconic orogeny: A correlative of the Annieopsquotch ophiolite belt of central Newfoundland?: Journal Geological Society of London, v. 170, p. 861–876.

——2013b, Stratigraphic, geochemical and U-Pb zircon constraints from Slieve Gallion, Northern Ireland: A correlation of the Irish Caledonian arcs: Journal Geological Society of London, v. 170, p. 737–752.

Hollis, S.P., Roberts, S., Earls, G., Herrington, R., Cooper, M.R., Piercey, S.P., Archibald, S.M., and Moloney, M., 2014, Petrochemistry and hydrothermal alteration within the Tyrone Igneous Complex, Northern Ireland: Implications for VMS mineralization in the British and Irish Caledonides: Mineralium Deposita, v. 49, p. 575–593.

Jourdan, F., Verati, C., and Feraud, G., 2006, Intercalibration of the Hb3gr $^{40}Ar/^{39}Ar$ dating standard: Chemical Geology, v. 231, p. 177–189.

Kirkland, C.L., Alsop, G.I., Daly, J.S., Whitehouse, M.J., Lam, R., and Clark, C., 2013, Constraints on the timing of Scandian deformation and the nature of a buried Grampian terrane under the Caledonides of northwestern Ireland: Journal Geological Society of London, v. 170, p. 615–625.

Kirkpatrick, J.D., Dobson, K.J., Mark, D.F., Shipton, Z.K., Brodsky, E.E., and Stuart, F.M., 2012, The depth of pseudotachylyte formation from detailed

thermochronology and constraints on coseismic stress drop variability: Journal of Geophysical Research B: Solid Earth, v. 117 (6), art. B06406.
Lawley, C.J.M., and Selby, D., 2012, Re-Os geochronolgy of quartz-enclosed ultrafine molybdenite: Implications for ore geochronolgy: Economic Geology, v. 107, p. 1499–1505.
Lawther, S.E.M., and Moloney, M., 2012, Curraghinalt gold deposit, County Tyrone, N. Ireland [abs.]: Transactions Institution Mining Metallurgy, sec. B, v. 121, p. 189.
Lee, J-Y., Marti, K., Severinghaus, J.P., Kawamura, K., Yoo, H.S., Lee, J.B., and Kim, J.S., 2006, A redetermination of the isotopic abundances of atmospheric Ar: Geochimica et Cosmochimica Acta, v. 70, p. 4507–4512.
Mark, D.F., Parnell, J., Kelley, S.P., Lee, M., Sherlock, S.C., and Carr, A., 2005, Dating of multistage fluid flow in sandstones: Science, v. 309, p. 2048–2051.
Mark, D.F., Parnell, J., Kelley, S.P., and Sherlock, S.C., 2006, Temperature-composition-time (TXt) data from authigenic K-feldspar: An integrated methodology for dating fluid flow events: Journal of Geochemical Exploration, v. 89, p. 256–292.
Mark, D.F., Kelley, S.P., Sherlock, S.C., Parnell, J., Lee, M.R., and Brown, D., 2008, Ar-Ar dating of authigenic K-feldspar: Quantitative modeling of radiogenic argon loss through subgrain boundary networks: Geochimica et Cosmochimica Acta, v. 72, p. 2695–2710.
Mark, D.F., Barfod, D.N., Stuart, F.M., and Imlach, J.G., 2009, The ARGUS multicollector noble gas mass spectrometer: Performance for $^{40}Ar/^{39}Ar$ geochronology: Geophysics Geochemistry Geosystems, v. 10, p. 1–9.
Mark, D.F., Parnell, J., Kelley, S.P., Lee, M.R., and Sherlock, S.C., 2010a, Dating of oil generation and migration at complex continental margins: Geology, v. 38, p. 75–78.
Mark, D.F., Gonzalez, S., Huddart, D., and Bohnel, H., 2010b, Dating of the Valsequillo volcanic deposits: Resolution of an ongoing controversy in Central Mexico: Journal of Human Evolution, v. 58, p. 441–445.
Mark, D.F., Rice, C.M., Lee, M.R., Fallick, A.E., Boyce, A., Trewin, N.H., and Lee, J.K.W., 2011a, $^{40}Ar/^{39}Ar$ dating of hydrothermal activity, biota and gold mineralization in the Rhynie hot-spring system, Aberdeenshire, Scotland: Geochimica et Cosmochimica Acta, v. 75, p. 555–569.
Mark, D.F., Stuart, F.M., and de Podesta, M., 2011b, New high-precision measurements of the isotopic composition of atmospheric argon: Geochimica et Cosmochimica Acta, v. 75, p. 7494–7501.
Mark, D.F., Petraglia, M., Smith, V.C., Morgan, L.E., Barfod, D., Ellis, B., Pearce, N.J., Pal, J.N., and Korisettar, R., 2014, A high precision Ar/Ar age for the young Toba Tuff and dating of ultra-distal tephra: Forcing of quaternary climate and implications for hominin occupations if India: Quaternary Geochronology, v. 21, p. 90–103, doi:10.1016/j.quageo.2012.12.004.
McCaffrey, K.J.W., and Johnston, J.D., 1996, Fractal analysis of a mineralised vein deposit: Curraghinalt gold deposit, County Tyrone: Mineralium Deposita, v. 31, p. 52–58.
Menzies, C.D., Teagle, D.A.H., Craw, D., Cox, S.C., Boyce, A.J., Barrie, C.D., and Roberts, S., 2014, Incursion of meteoric waters into the ductile regime in an active orogen: Earth and Planetary Science Letters, v. 399, p. 1–13.
Mitchell, W.I., 1977, The Ordovician Brachiopoda from Pomeroy, Co. Tyrone: Palaeontological Society of London Monograph, v. 130, 138 p.
Moore, J., Kuhn, B., Mark, D.F., and Tsikos, H., 2011, A sugilite-bearing assemblage from the Wolhaarkop breccia, Bruce mine, South Africa: Evidence for alkali metasomatism: Journal of European Mineralogy, v. 23, p. 661–673.
Oliver, G.J.H., 2001, Reconstruction of the Grampian episode in Scotland: Its place in the Caledonian orogeny: Tectonophysics, v. 332, p. 23–49.
Parnell, J., Earls, G., Wilkinson, J.J., Hutton, D.H.W., Boyce, A.J., Fallick, A.E., Ellam, R.M., Gleeson, S.A., Moles, N.R., Carey, P.F., Legg, I., and Carey, P.F., 2000, Regional fluid flow and gold mineralization in the Dalradian of the Sperrin Mountains, Northern Ireland: Economic Geology, v. 95, p. 1389–1416.
Power, S.E., Ryan, P.D., and Feely, M., 2001, Fluid inclusion studies on the late structural history of the Connemara Dalradian, western Ireland [abs.]: Geological Society America Abstracts with Program, v. 33, A448.
Renne, P.R., 2014, Some footnotes to the optimization-based calibration of the $^{40}Ar/^{39}Ar$ system: Geological Society of London Special Publication 378, http://dx.doi.org/10.1144/sp378.17.
Renne, P.R., Swisher, C.C., Deino, A.L., Karner, D.B., Owens, T.L., and DePaolo, D.J., 1998, Intercalibration of standards, absolute ages and uncertainties in $^{40}Ar/^{39}Ar$ dating: Chemical Geology, v. 145, p. 117–152.
Renne, P.R., Deino, A.L., Hames, W.E., Heizler, M.T., Hemming, S.R., Hodges, K.V., Koppers, A.A.P., Mark, D.F., Morgan, L.E., Phillips, D., Singer, B.S., Turrin, B.D., Villa, I.M., Villeneuve, M., and Wijbrans, J.R., 2009, Data reporting norms for $^{40}Ar/^{39}Ar$ geochronology: Quaternary Geochronology, v. 4, p. 346–352.
Renne, P.R., Mundil, R., Balco, G., Min, K., and Ludwig, K.R., 2010, Joint determination of ^{40}K decay constants and $^{40}Ar^*/^{40}K$ for the Fish Canyon sanidine standard, and improved accuracy for $^{40}Ar/^{39}Ar$ geochronology: Geochimica et Cosmochimica Acta, v. 74, p. 5349–5367.
Renne, P.R., Balco, G., Ludwig, K.R., Mundil, R., and Min, K., 2011, Response to comment by Schwarz, W.H. et al. on "Joint determination of ^{40}K decay constants and $^{40}Ar^*/^{40}K$ for the Fish Canyon sanidine standard, and improved accuracy for $^{40}Ar/^{39}Ar$ geochronology": Geochimica et Cosmochimica Acta. v. 75, p. 5097–5100.
Renne, P.R., Deino, A.L., Hilgen, F.J., Kuiper, K.F., Mark, D.F., Mitchell, W.S., III, Morgan, L.E., Mundil, R., and Smit, J., 2013, Time scales of critical events around the Cretaceous-Paleogene boundary: Science, v. 339, p. 684–687.
Selby, D., and Creaser, R.A., 2001, Re-Os geochronology and systematics in molybdenite from the Endako porphyry molybdenum deposit, British Columbia, Canada: Economic Geology, v. 96, p. 197–204.
——2004, Macroscale NTIMS and microscale LA-MC-ICP-MS Re-Os isotope analysis of molybdenite: Testing spatial restrictions for reliable Re-Os age determinations and implications for the decoupling of Re-Os within molybdenite: Geochimica et Cosmochimica Acta, v. 68, p. 3897–3908.
Selby, D., Creaser, R.A., Hart, C.J.R., Rombach, C.S., Thompson, J.F.H., Smith, M.T., Bakke, A., and Goldfarb, R.J., 2002, Absolute timing of sulphide and gold mineralization: A comparison of Re-Os molybdenite and Ar/Ar mica methods from the Tintina gold belt, Alaska: Geology, v. 30, p. 791–794.
Soper, N.J., Ryan, P.D., and Dewey, J.F., 1999, Age of the Grampian orogeny in Scotland and Ireland: Journal Geological Society of London, v. 156, p. 1231–1236.
Standish, C.D., Dhuime, B., Chapman, R.J., Hawkesworth, C.J., and Pike, A.W.G., 2014, The genesis of gold mineralization hosted by orogenic belts: A lead isotope investigation of Irish gold deposits: Chemical Geology, v. 378, p. 40–51.
Steiger, R.H., and Jäger, E., 1977, Subcommission on geochronology: Convention on the use of decay constants in geo- and cosmochronology: Earth and Planetary Science Letters, v. 36, p. 359–362.
Strachan, R.A., Smith, M., Harris, A.L., and Fettes, D.J., 2002, The Northern Highland and Grampian terranes, *in* Trewin, N.H. ed., The geology of Scotland: Geological Society of London, p. 81–147.
Suzuki, K., 1996, Re-Os dating of molybdenites from ore deposits in Japan: Implications for the closure temperature of the Re-Os system for molybdenite and the cooling history of molybdenum ore deposits: Geochimica et Cosmochimica Acta, v. 64, p. 223–232.
Volkening, J., Walczyk, T., and Heumann, K.G., 1991, Osmium isotope ratio determinations by negative ion mass spectrometry: International Journal of Mass Spectrometry Ion Processes, v. 105, p. 147–159.
Weatherly, D.K., and Henley, R.W., 2013, Flash vaporization during earthquakes evidenced by gold deposits: Nature Geoscience, v. 6, p. 294–298.
Wheeler, J., 1996, "Diffarg," a program for simulating argon diffusion in minerals: Computers & Geosciences, v. 22, p. 919–929.
Wilkinson, J.J., Boyce, A.J., Earls, G., and Fallick, A.E., 1999, Gold remobilization by low-temperature brines: Evidence from the Curraghinalt gold deposit, Northern Ireland: Economic Geology, v. 94, p. 289–296.
Yardley, B.W.D., and Cleverly, J.S., 2013, The role of metamorphic fluids in the formation of ore deposits: Geological Society of London Special Publication 393, Online First, doi 10.1144/SP393.5.
Yardley, B.W.D., and Graham, J.T., 2002, Origins of salinity in metamorphic fluids: Geofluids, v. 2, p. 249–256.